POLITECNICO DI TORINO
Repository ISTITUZIONALE

Analysis of the influence of passenger vehicles front-end design on pedestrian lower extremity injuries by means of the LLMS model

Original
Analysis of the influence of passenger vehicles front-end design on pedestrian lower extremity injuries by means of the LLMS model / Scattina, A., Mo, F., Masson, C., Avalle, M., Arnoux Pierre, J.. - In: TRAFFIC INJURY PREVENTION. - ISSN 1538-9588. - STAMPA. - 19:5(2018), pp. 535-541. [10.1080/15389588.2018.1432858]

Availability:
This version is available at: 11583/2715876 since: 2018-10-29T09:33:25Z

Publisher:
Taylor & Francis

Published
DOI:10.1080/15389588.2018.1432858

Terms of use:

This article is made available under terms and conditions as specified in the corresponding bibliographic description in the repository

Publisher copyright
Taylor and Francis postprint/Author's Accepted Manuscript

This is an Accepted Manuscript of an article published by Taylor & Francis in TRAFFIC INJURY PREVENTION on 2018, available at http://wwww.tandfonline.com/10.1080/15389588.2018.1432858

(Article begins on next page)

13 November 2026

Analysis of the influence of passenger vehicles front-end design on pedestrian lower extremity injuries by means of the LLMS model

Alessandro Scattina[a*], Fuhao Mo[b,c], Catherine Masson[c], Massimiliano Avalle[d], Pierre Jean Arnoux[b]

[a] Mechanical and Aerospace Engineering Department, Politecnico di Torino, Torino, Italy

[b] State Key Laboratory of Advanced Design and Manufacture for Vehicle Body, Hunan University, Changsha, China

[c] Laboratoire de Biomécanique Appliquée (IFSTTAR-AIX-Marseille Université), Marseille, France

[d] Department of Mechanical, Energy, Management and Transport Engineering, Università degli Studi di Genova, Genova, Italy

Email addresses:

Alessandro Scattina: alessandro.scattina@polito.it

Fuhao Mo: fuhaomo@hnu.edu.cn

Catherine Masson: catherine.masson@ifsttar.fr

Massimiliano Avalle: massimiliano.avalle@unige.it

Pierre Jean Arnoux: pierre-jean.arnoux@ifsttar.fr

***Corresponding author:**

Alessandro Scattina

Politecnico di Torino, Department of Mechanical and Aerospace Engineering

Corso Duca degli Abruzzi 24, 10129 Torino, Italy

Tel: +39 0110906900

Fax: +39 0110906999

E-mail: alessandro.scattina@polito.it

Analysis of the influence of passenger vehicles front-end design on pedestrian lower extremity injuries by means of the LLMS model

ABSTRACT

Objective: The work aims at investigating the influence of some front-end design parameters of a passenger vehicle on the behavior and damage occurring in the human lower limbs while impacted in an accident.

Methods: The analysis is carried out by means of finite element analysis using a generic car model for the vehicle and the Lower Limbs Model for Safety (LLMS) for the purpose of pedestrian safety. Considering the pedestrian standardized impact procedure (as in the 2003/12/EC Directive) a parametric analysis, through a DOE plan, was done. Various material properties, bumper thickness, position of the higher and lower bumper beams and the position of pedestrian, were made variable in order to identify how they influence the injury occurrence. The injury prediction was evaluated from the knee lateral flexion, the ligaments elongation, and the state of stress in the bone structure.

Results: The results highlighted that the offset between the higher and lower bumper beams is the most influencing parameter affecting the knee ligament response. The influence is smaller or absent considering the other responses and the other considered parameters. The stiffness characteristics of the bumper are, instead, more notable on the tibia. Even if an optimal value of the variables could not be identified trends were detected, with the potential of indicating strategies for improvement.

Conclusions: The behavior of a vehicle front-end in the impact against a pedestrian can be improved optimizing its design. The work indicates potential strategies for improvement. In this work, each parameter was changed independently one at a time: in future works the interaction between the design parameters could be also investigated. Moreover, a similar parametric analysis can be carried out using a standard mechanical legform model in order to understand potential diversities or correlations between standard tools and human models.

KEYWORDS: finite element model; pedestrian safety; lower limb; knee ligaments; tibia; front-end design

INTRODUCTION

During the past three decades, injury biomechanics in vehicle-pedestrian collisions has been extensively studied. On the basis of several analysis of accidental data, passenger vehicles were proven to be responsible for most pedestrian injuries (Mallory and Stammen 2006; Gavrila et al. 2003). Pedestrian lower extremities are the most frequently injured body region (IHRA 2001; Cater et al. 2008) and the injury analyses have been continuously addressed by researchers by using both experimental tests and finite element simulations (Arnoux et al. 2005; Yasuki 2007; Mo et al. 2012; Mo et al. 2015, Masson et al. 2007; Kerrigan et al. 2008).

To this aim, the European Enhanced Vehicle-safety Committee (EEVC WG17 1998; EEVC WG10 1994) proposed a series of subsystem impactor tests to evaluate the aggressiveness of passenger vehicles with respect to pedestrians. Based on these proposals, the European Commission Directive 2003/102/EC enacted a lower-leg impactor test procedure to improve passenger vehicles design and mitigate pedestrian lower extremity injuries. This test procedure uses a mechanical legform developed by the Transport Research Laboratory (TRL) to represent the lower extremity of the human body. Many studies have addressed the problems of both the legform

and injury criteria used in this test procedure (Yasuki 2007; Mo, Arnoux, Cesari and Masson 2012; Yasuki 2007; Mo, Arnoux, Jure and Masson 2012; Martinez et al. 2008). After this, the Japan Automobile Research Institute (JARI) and the Japan Automobile Manufacturer Association (JAMA) developed a Flexible Pedestrian Legform Impactor (Flex-PLI). The Flex-PLI has flexible tibia and femur components mainly made of a high strength plastic with a fiber reinforced bone inside. The knee component is also flexible with four major ligaments made of springs and stainless steel wires. The elongation of the ligaments was measured to evaluate potential knee injuries in the legform. Global technical regulation No.9 of the Economic Commission for Europe (ECE) presented the application of Flex-PLI for the pedestrian protection (Committee 2010).

In order to guide the improvement of passenger vehicle design for pedestrian protection, all these legform tests should be available to reflect real-world impact environments. Thus, the full-scale vehicle-pedestrian impact test is the basis for the development and improvement of these regulatory tests. Moreover, supported by the current development of computer modeling, full-scale vehicle-pedestrian impacts can be performed by means of numerical simulations with a much lower cost if compared to the experimental methods. With the Finite Element (FE) simulations, it is possible to focus the attention only on the most interesting sequences of the full scale tests. Moreover, the numerical simulations allow to study the influence of many different design parameters, reducing times and costs if compared to the real experimental tests. Large DOE analysis can be carried out and consequently it is possible to define an accurate hierarchy of the most important design parameters concerning the pedestrian injuries. To this aim, the influence of the vehicle front-end structures on the pedestrian kinematics and the pedestrian injuries were studied in many works in the past (for a detailed analysis of the previous works see the literature review in the Appendix).The goal of the present study is to investigate in more details the influence of some design parameters of a vehicle front-end structure on the injuries of the lower extremity of the pedestrians.

MODELS AND METHODS

FE Models

Vehicle-pedestrian impacts (Figure 1) were simulated in order to investigate the influence of the design parameters of a passenger vehicle front-end design on the pedestrian lower extremity injuries. The vehicle was simulated with one of the GCMs (Generic Car Models) developed within the APROSYS EU FP7 funded project (APROSYS 2011). In particular, in this work, the GCM4 vehicle was used. It is the model of an MPV. The initial vehicle model was slightly modified to include the nowadays usual two load lines, upper and lower, as shown in Figures 2 and A1. In front of these elements, there is the usual plastic bumper fascia. In this work, to reduce the computational time, only the front part of the vehicle model was used (Figures 1 and A1).

The pedestrian was simulated combining a 50% Hybrid III dummy and a biofidelic lower limb model known as *Lower Limb Model for Safety* (LLMS, Arnoux 2000; Beillas et al. 2001; Arnoux et al. 2005) shown in Figures 1 and 2. The Hybrid III model and the LLMS model are joined together at the hip joint: the right leg is modelled by the LLMS whereas the left leg is a normal dummy leg model. The Hybrid III model was used to consider the human body mass and the inertia effects during the simulations without taking into consideration tissue damage and failure. For the other leg, the LLMS was used as a tool to study the injuries caused by the vehicle impact. In order to simulate the pedestrian in walking condition, the left leg of the pedestrian model, the one that belongs to the Hybrid III model, was in contact with the ground. The right leg of the pedestrian model, the one including the

LLMS model, was raised with respect to the ground of a small step to equalize the legs height, as shown in Figure 2. More details about the GCM4 and the LLMS models can be found in the Appendix.
All the impacts were along the transverse direction with respect to the leg, with the vehicle traveling at a fixed speed of 40 km/h.

Geometrical and Material Parameters Investigated

Design variations were of three types:

- Geometrical
- Test conditions (positioning of the leg with respect to the front-end)
- Materials (influence of the stiffness)

As illustrated in Figures 1 and 2, five different geometrical parameters can be changed defining the interface between vehicle front-end and pedestrian, plus one position parameter. These parameters are:

1. a higher absorber depth (in the longitudinal X direction)
2. d longitudinal offset between upper and lower load line
3. h vertical distance between upper and lower load line
4. p vertical distance between the upper load line and the knee
5. z vertical height of the foot bottom with respect to the ground
6. Y transverse offset of the knee with respect to a reference plane

As shown in Figure 1 and A2, the transverse offset influences the impact condition because in the $Y = -125$ mm position the impactor is near the edge of the absorber whereas in the offset $Y = 0$ mm (reference) position the impactor is facing the central zone. A different behavior was expected due to the different stiffness of the absorber in these two positions.
Even if there are five geometrical parameters, only four were considered as variables in the current analysis since the z parameter is only an auxiliary offset used to position the leg with respect to different vehicles as done in Mo et al. (2015). In the present analysis there is only one vehicle and the two vertical distances h and p are the two degrees of freedom necessary and sufficient to define and analyze the impact situation along the vertical direction. The reference values and the range of the parameters were defined on the base of the geometry of the vehicle model adopted for the analysis and considering the geometries of the best-in-class multipurpose vehicles currently available.
The four possible material parameters were:

1. e the thickness of the bumper fascia
2. E the elastic modulus of the bumper fascia
3. E_h the elastic modulus of the material of the higher load line (higher absorber)
4. E_l the elastic modulus of the material of the lower load line (lower absorber)

In the current work, only the elastic modulus of the bumper fascia E was not included in the analysis: in a preliminary analysis it showed little influence on the phenomenon, because the load transferred to the leg is primarily generated by the absorbers. In the Table 1 the numerical variations of the considered parameters are summarized.

Measured Biomechanical Parameters

Tibia bending moments and knee ligament strains were measured to evaluate the injury risk of the knee structure. Tibia bending moments of different regions were measured in sections defined at approximately each layer of the tibia elements along its axial direction (Figure A3). The ligaments strains were measured evaluating the strains of several springs. The ligament was considered failed when the value of the engineering strain of the entire ligament exceeded its defined strain threshold. More details about the evaluation of the ligament strains from a numerical point of view can be found in the Appendix. The thresholds of the ligament failure adopted in this work were based on experimental results and validated through complex loading conditions (Arnoux et al. 2002). The ultimate strains for the collateral ligaments were considered between 25% and 38% whereas the limit values for the cruciate ligaments were considered between 18% and 24%. As proposed by Mo et al. (2014), in this work, the threshold of the strain level for the cruciate ligaments was fixed to 24% whereas the threshold of the strain level for the collateral ligaments was fixed to 28%.

To determine the influence of the examined parameters on the injury occurrences of the tibia and knee ligaments, the lower extremities kinematics were also recorded by taking the positions of several nodes along the tibia and femoral axes (Figure A5).

Simulation Plan

The analysis of the problem as discussed above resulted in a simulation plan based on seven variables. Namely, they were:

1. Y transverse offset of the knee with respect to a reference plane
2. d longitudinal offset between upper and lower load line
3. h vertical distance between the upper and lower load line
4. p vertical distance between the upper load line and the knee
5. e the thickness of the bumper fascia
6. E_h the elastic modulus of the higher load line material (higher absorber)
7. E_l the elastic modulus of the lower load line material (lower absorber)

With the exception of the transverse offset Y, all the remaining parameters were changed independently one at a time with respect to the 0 level (reference values, as reported in Tables 1). On the contrary, the whole set of simulations by changing the remaining parameters were repeated for the two Y levels of 0 and −125 mm.

This brings out a total of (1 reference + 6 variations in d + 5 × 2 other variations) × 2 = 34 simulations (the latter multiplier related to the variation of the transverse offset Y).

RESULTS

Lower Limb Kinematics

A first analysis of the kinematics of the leg during the impact (Figures A6 and A7) reveals that at least two parameters have very little or even negligible influence, namely the distance h between the higher (absorber) and lower line, and the thickness of the bumper fascia e. There is also a little influence of the elastic moduli. As shown in the figures, the more influencing factors are geometrical, and they are the vertical distance between the upper load line and the knee p and, even more important, the longitudinal offset d between the upper and lower load line. A more advanced position of the lower line increases the displacements of the lower leg.

This analysis will give some first general indications on the leg behavior, but a more advanced and detailed analysis will derive from the evaluation of strain in the ligaments and tibia bending.

Knee Ligaments

At a first glimpse, it appears (Figures A8 and A9) that the MCL is the more sensitive to almost every parameter: this is expected due to the type of impact, since the MCL suffers mainly from the bending generated in the accident. This is especially evident in the case of the central position ($Y = 0$) whereas in the transverse offset position the effect is more evident and more marked while varying the longitudinal offset d and the elastic moduli only. Similar considerations can be done for the PCL and ACL ligaments, whereas the LCL is almost unaffected by any parameter. In particular, considering the PCL ligament, when the leg is in the central position ($Y = 0$), all the parameters had a certain effect on the strain, whereas, when the leg is in the $Y = -125$ mm only a change in the h parameter and in the elastic moduli influences the ligament strain. Moreover, the reduction of the Young modulus of the higher line seems to bring a significant reduction of strains. For the ACL ligament, reducing the p parameters allows also a consistent reduction in the ligament strains as the reduction of the elastic modulus of the higher load line does; the longitudinal offset d has instead a moderate influence.

Bending

Examining the bending moments as a function of the tibia position (Figures A10 and A11) it is interesting to observe that some parameters have a strong influence on the bending behavior. In particular, it is noticeable that in some cases the position of the maximum bending point moves toward the knee: consequently, the lower part of the tibia is less stressed. This probably means that there will be a change in the fracture position of the tibia. A change in the offset d, affects not only the position of the maximum bending moment but also its maximum value. Negative values of d give higher values of the maximum bending moment. At the same time, an increase of the offset d moves the maximum bending point toward the foot, the tibia is less stressed but more evenly. The other parameters considered have an influence only on the position of the maximum bending moment, whereas the maximum values remain quite constant. The only geometrical parameters without significant influence on the bending moment is the distance h: in this case, all the curves are very similar. Considering the thickness of the bumper fascia e, a decrease of its value moves the position of the maximum bending moment toward the knee. A similar trend was also obtained with an increase of the vertical distance between the upper load line and the knee p. About the materials, only the elastic modulus of the higher load line had a significant influence on the results: reducing it, the position of the maximum bending moment moves toward the knee. Similar trends were also obtained considering the offset leg position $Y = -125$ mm. In this case, generally, the position of the maximum bending moves toward the foot if compared with the results obtained in $Y = 0$.

Examining the trend of the maximum value of the bending moment as a function of the simulation time (Figures A10 and A11), considering both leg positions, it is observed that only the longitudinal offset d had a small influence on this value. Decreasing the distance d, the maximum bending increases, but for a higher simulation time. The other examined parameters had no influence: the curves are very similar in all other considered cases. A slight decrease of the moment can be observed, in the first part of the impact, using a value of $h = 280$ mm.

Factorial and Regression Analysis

A factor analysis (Jolliffe 1986) of the results in term of the time corresponding to the maximum values of the examined output (Table 2) and in terms of the maximum values of the considered output results (Table 3) was carried out.

In the correlation matrix of Table 2, the larger values reveal the parameters having a higher influence on the output. The longitudinal distance *d* between the higher and the lower line had the higher influence on timing for the maximum bending moment in the tibia. On the other hand, all the values of the time at the maximum strains are more influenced by the vertical distance *p* between the knee and the upper load line and, secondarily, by the elastic modulus E_h of the material of the higher load line.

A linear regression analysis gives the expressions for the relations between the input variables and the considered outputs shown in Eq. (1). The most significant influences are summarized in Figure 3 and A12 (left hand sides).

$$
\begin{aligned}
t\left(M_{t,\max}\right) &= \left(42.4 + 0.0276Y + 0.130p + 0.128h - 0.230d - 31.9e - 4.69\times10^{-3}E_h - 5.62\times10^{-3}E_l\right)ms \\
t\left(\varepsilon_{MCL,\max}\right) &= \left(25.0 - 0.0071Y - 0.128p + 0.0265h - 0.0277d - 0.350e - 4.73\times10^{-3}E_h + 7.81\times10^{-3}E_l\right)ms \\
t\left(\varepsilon_{PCL,\max}\right) &= \left(-10.3 - 0.0272Y - 0.305p + 0.132h + 0.0334d + 4.70e - 7.54\times10^{-3}E_h + 3.01\times10^{-3}E_l\right)ms \\
t\left(\varepsilon_{ACL,\max}\right) &= \left(37.7 - 0.00729Y - 0.148p + 0.138h + 0.00239d + 0.0500e - 12.1\times10^{-3}E_h + 0.352\times10^{-3}E_l\right)ms \\
t\left(\varepsilon_{LCL,\max}\right) &= \left(18.6 - 0.0191Y + 0.271p + 0.0462h - 0.0491d - 2.10e - 6.64\times10^{-3}E_h + 0.973\times10^{-3}E_l\right)ms
\end{aligned}
\qquad (1)
$$

From the results of the factor analysis of Table 3, it comes out that the most influencing factor on the maximum value of the tibia moment M_t is clearly the longitudinal distance *d* between the higher and the lower line, followed by the vertical distance *h* between the upper and the lower load line. About the maximum values of the ligament strains, the situation is slightly more complicated. The most influencing factor can be considered again the longitudinal distance *d* between the higher and the lower line, but the second most influencing factor is in some case the transverse offset of the knee *Y* and in some other cases the vertical distance between the upper load line and the knee *p.* Moreover, these effects are not always of the same sign. On the contrary, the effect of the longitudinal distance *d* is always negative, that is an increase of *d* gives a decrease of all the output results.

A linear regression analysis gives the expressions for the relations between the input variables and the considered maximum values of the output results shown in Eq. (2). These results are plotted (Figure 3 and A12, right hand sides) showing the effect of the most influencing variables.

$$
\begin{aligned}
M_{t,\max} &= \left(343.3 - 0.02464Y - 0.07006p - 0.6419h - 0.8283d + 0.1183e + 12.5\times10^{-3}E_h - 2.29\times10^{-3}E_l\right)Nm \\
\varepsilon_{MCL,\max} &= 1.646 + 0.682\times10^{-3}Y - 5.37\times10^{-3}p - 1.41\times10^{-3}h - 4.28\times10^{-3}d - 19.8\times10^{-3}e - 4.98\times10^{-6}E_h - 34.9\times10^{-6}E_l \\
\varepsilon_{PCL,\max} &= 1.416 + 0.844\times10^{-3}Y - 2.29\times10^{-3}p - 1.74\times10^{-3}h - 1.40\times10^{-3}d - 29.3\times10^{-3}e + 80.3\times10^{-6}E_h - 7.26\times10^{-6}E_l \\
\varepsilon_{ACL,\max} &= 0.660 - 0.269\times10^{-3}Y + 2.72\times10^{-3}p + 252\times10^{-3}h - 0.794\times10^{-3}d - 59.5\times10^{-3}e + 8.43\times10^{-6}E_h + 2.18\times10^{-6}E_l \\
\varepsilon_{LCL,\max} &= 0.596 - 0.212\times10^{-3}Y - 5.05\times10^{-3}p - 0.105\times10^{-3}h - 2.80\times10^{-3}d - 8.95\times10^{-3}e - 15.1\times10^{-6}E_h + 17.8\times10^{-6}E_l
\end{aligned}
$$

(2)

DISCUSSION

From the sensitivity analysis proposed above, it seems that the injury mechanisms of the leg had no relevant changes in the cases examined. However, some parameters seem to modify the location of the injury, by modifying the position of the bending moment along the tibia. Consequently, the time for injury occurrence could also

change. A delay in the injury time is usually considered a positive circumstance for safety, because it offers more possibilities to work in collaboration with active safety devices.

Considering the regression analysis, even if the linear models adopted in both cases are a rough approximation of the outputs, they can be considered anyway as a valid estimator of them. This is both because of the limited range of variation of most considered variables and to the small number of levels for some variables not allowing for a more detailed description. Adopting higher level of approximations is useless (as it is clear from Figure 3 there are not clear trends that can be interpreted differently, justified also by the R-squared values of the approximation which are always greater than 0.5) and even misleading: local variations due to the high non-linearity of the problem, if any, are not to be considered when searching for general trends to establish design rules as in this case.

For what concerns the design of the car front end, it appears, as expected, that the geometry and the stiffness properties of the bumper, are important factors. These parameters affect the behavior and damage occurring in the leg during a pedestrian accident. On the whole, it appears that it is the longitudinal offset between the upper and the lower load line d that plays the greater role. This important result is confirmed both by field studies by Li, Lyons, Wang, Yang, Otte and Haasper (2007) who found the bumper lower depth (horizontal) as a most affecting parameter on leg injury risk and by computational studies by Li, Yang and Simms (2017) who concluded that a smaller longitudinal difference between the higher and lower profile of the front end is beneficial in terms of injury risk. This is probably because the offset impact along the leg induces a strong rotation with consequent larger loads and strains. Apparently, but not expectedly, the vertical positions and the distance of the upper and the lower load line have a lesser influence: probably the considered variations, chosen in a reasonable range for the current application, are not enough to change noticeably the kinematics, and thus, the damage on the leg. This is partially consistent, but not in contrast, with the results again shown by Li, Lyons, Wang, Yang, Otte and Haasper (2007) and Li, Yang and Simms (2017) and confirmed by other researches even based on much detailed data not convincingly showing that the height of the bumper influences the location of the injuries (Martin et. al 2011; Otte and Haasper. 2007). Similarly, Zhang et al. (2008) did not acknowledge the car front-end height with lower extremity injury odds.

The transverse position is also affecting but this result is not conclusive since the actual detailed shape and local stiffness of the beam must be considered. As demonstrated also by Dunmore et al. (2006) and by Liu et al. (2002), the bumper stiffness, expressed in this work by the thickness of the fascia and the elastic moduli of the two load lines, moderately affects the damage on the ligaments but has a slightly higher effect on the tibia bone. This is probably because of the different mechanical behavior: the bone is much stiffer than the ligaments.

This analysis confirms how the design choices for the front-end of a car are very important for the reduction of pedestrian injuries in case of impact. It clearly emerges that a soft uniform front structure can mitigate the severity of the injuries. In more details, it appears that, in some cases, the reference values of the parameters considered brings to the lower loads or stresses obtained: this highlights that those values can be considered as optimal.

ACKNOWLEDGMENTS

The authors wish to thank Elena Semino for her contribution to this work.

REFERENCES

Abvabi A, Nasr A, Noorpoor A, Saeed Kiasat M. Investigation on the effect of impact location height on pedestrian safety using a legform impactor dynamic model. *Saf Sci*. 2010;48(5):660–671.

Abvabi A, Nasr A, Noorpoor A, Saeed Kiasat M. Lower extremity injuries in vehicle-pedestrian collisions using a legform impactor model. *J Zhejiang Univ Sci*. 2010;11:97–105.

APROSYS report summary, record number 47920, http://cordis.europa.eu/result/rcn/47920_en.html. Accessed October 24, 2017.

Arnoux PJ. Modélisation des ligaments des membres porteurs. Ph.D. Thesis. Université de la Méditerranée, 2000.

Arnoux PJ, Cesari D, Behr M, Thollon L, Brunet C. Pedestrian lower limb injury criteria evaluation: a finite element approach. *Traffic Inj Prev*. 2005;6(3):288–297.

Avalle M, Belingardi G, Ibba A. Stochastic crash analysis of vehicle models for sensitivity analysis and optimization. Paper presented at: 20th International Technical Conference on the Enhanced Safety of Vehicles (ESV); June 18–21, 2007; Lyon, France.

Belytschko T, Black T. Elastic crack growth in finite elements with minimal remeshing. *Int J Numer Methods Eng*. 1999;45:601–620.

Beillas P, Begeman PC, Yang KH, et al. Lower limb: advanced FE model and new experimental data. *Stapp Car Crash J*. 2001;45:469–494.

Cater EL, Neal-Sturgess CE, Hardy RN. APROSYS in-depth database of serious pedestrian and cyclist impacts with vehicles. *Int J Crashworthiness*. 2008;13(6):629–642.

Cheon SS, Choi JH, Lee DG. Development of the composite bumper beam for passenger cars. *Compos Struct*. 1995;32(1–4):491–499.

Committee ECfEIT. Proposal for amendments to global technical regulation No. 9. Geneva 2010.

Davoodi MM, Sapuan SM, Yunus R. Conceptual design of a polymer composite automotive bumper energy absorber. *Mater and Des*. 2008;29:1447–1452.

Dunmore MC, Brooks R, Madeley NJ, McNally DS. The effect of leg fracture level and vehicle front-end geometry on pedestrian knee injury and response. *Proc Inst Mech Eng H*. 2006;220(8):857–869.

Gavrila DM, Marchal P, Meinecke MM. Vulnerable road user scenario analysis. SAVE-U Project Deliverable 1-A. 2003.

European Experimental Vehicles Committee: Working Group 17 on Pedestrian Protection. Improved test methods to evaluate pedestrian protection afforded by passenger cars. 1998.

European Experimental Vehicles Committee: Working Group 10 on Pedestrian Protection. Proposals for methods to evaluate pedestrian protection for passenger cars: Final report. Australia 1994.

Harris J, Grew ND. *The influence of car design on pedestrian protection*. Society of Automotive Engineers, Warrendale, PA; 1985. SAE 856116.

Huang TJ, Wu JT, Hsiao CY, Wang MS, Lee KC. Design of a bumper system for pedestrian lower-leg protection using the Taguchi method. *Proc Inst Mech Eng D*. 2011;225(12):1578–1586.

International Harmonized Research Activities (IHRA). Pedestrian safety working group 2001 report. 2001.

Ishikawa H, Yamazaki K, Ono K, Sasaki A. Current situation of pedestrian accidents and research into pedestrian protection in Japan. Paper presented at: 13th International Technical Conference on the Enhanced Safety of Vehicles (ESV); November 4–7, 1991; Paris, France.

lshikawa H, Kajzer J, Ono K, Sakurai M. Simulation of car impact to pedestrian lower extremity influence of different car-front shapes and dummy parameters on test results. Paper presented at: International Research Council on Biomechanics of Injury (IRCOBI) conference; September 9–11, 1992; Verona, Italy.

Jiang K, Yang J. Optimization of bumper system for pedestrian lower leg protection from vehicle impact. Paper presented at: 3rd International Conference on Digital Manufacturing & Automation (ICDMA); 31 July–2 August 2012; GuiLin, China.

Jolliffe IT. Principal Component Analysis. Springer-Verlag, 1986.

Kerrigan J, Rudd R, Subit D, Untaroiu C, Crandall JRR. Pedestrian lower extremity response and injury: A small sedan versus a large sport utility vehicle. Paper presented at: SAE 2008 World Congress & Exhibition; April 14–17, 2008, Detroit, Michigan, USA.

Lee YH, Joo YJ, Park JS, Kim YS, Yim HJ. Robust design optimization of frontal structures for minimizing injury risks of Flex Pedestrian Legform Impactor. *Int J Automot Tech*. 2014;15:757–764.

Li G, Lyons M, Wang B, Yang J, Otte D, Simms C. The influence of passenger car front shape on pedestrian injury risk observed from German in-depth accident data. *Acc Anal Prev*. 2017;101:11–21.

Li G, Yang J, Simms C. Safer passenger car front shapes for pedestrians: A computational approach to reduce overall pedestrian injury risk in realistic impact scenarios. *Acc Anal Prev*. 2017;100:97–110

Liu XJ, Yang JK, Lövsund P. A study of influences of vehicle speed and front structure on pedestrian impact responses using mathematical models. *Traffic Inj Prev*. 2002;3(1):31–42.

Liu W, Cheng X, Shan Y, Li H, Yang H. Improvement of bumper structure for pedestrian lower leg protection based on Euro-NCAP 2011. Paper presented at: International Conference on Mechatronic Science, Electric Engineering and Computer; August 19–22, 2011; Jilin, China.

Mallory A, Stammen J. Lower extremity pedestrian injury in the U.S.: A summary of PCDS data. NHTSA Vehicle Research and Test Center, 2006.

Martin J-L, Lardy A, Laumon B. Pedestrian injury patterns according to car and casualty characteristics in France. *Ann Adv Automot Med*. 2011;55:137–146.

Martinez L, Compigne S, Guerra LJ. Influence of vehicle shape and stiffness on the pedestrian lower extremity injuries: Review of current pedestrian lower leg test procedure. Paper presented at: International Research Council on Biomechanics of Injury (IRCOBI) conference; 17–19 September, 2008; Bern, Switzerland.

Masson C, Serre T, Cesari D. Pedestrian-vehicle accident: analysis of 4 full scale tests with PMHS. Paper presented at 20th International Technical Conference on the Enhanced Safety of Vehicles (ESV); June 18–21, 2007; Lyon, France.

Matsui Y. Effects of vehicle bumper height and impact velocity on type of lower extremity injury in vehicle–pedestrian accidents. *Accid Anal Prev*. 2005;37:633–40.

Mo F, Arnoux PJ, Avalle M, Scattina A, Semino E, Masson C. Incidences of various passenger vehicle front-end designs on pedestrian lower limb injuries. *Int J of Crashworthiness*. 2015;20(4):337–347.

Mo F, Arnoux PJ, Cesari D, Masson C. The failure modeling of knee ligaments in the finite element model. *Int J of Crashworthiness*. 2012;17(6):630–636.

Mo F, Arnoux PJ, Cesari D, Masson C. Investigation on the injury threshold of the knee ligaments by the parametric study of car-pedestrian impact conditions. *Saf Sci*. 2014;62:58–67.

Mo F, Arnoux PJ, Jure JJ, Masson C. Injury tolerance of tibia for the car–pedestrian impact. *Accid Anal Prev*. 2012;46(0):18–25.

Mo F, Arnoux PJ, Zahidi O, Masson C. Injury thresholds of the knee ligaments under lateral shear loadings: an experimental study. *Traffic Inj Prev*. 2013;14(6):623–629.

Mo F, Masson C, Cesari D, Arnoux PJ. Coupling lateral bending and shearing mechanisms to define knee injury criteria for pedestrian safety. *Traffic Inj Prev*. 2013;14(4):378–386.
Moon H, Jeon Y, Kim DY, Kim HY, Kim Y. Crumple zone design for pedestrian protection using impact analysis. *J Mech Sci Tech*. 2012;26(8):2595–2601.
Nagasaka K, Mizuno K, Tanaka E, Yamamoto S, Iwamoto M, Miki K, Kajzer J. Finite element analysis of knee injury risks in carto-pedestrian impacts. *Traffic Inj Prev*. 2003;4(4):345–354.
Niederer PF, Schlumpf MR. *Influence of vehicle front geometry on impacted pedestrian kinematics*. Society of Automotive Engineers, Warrendale, PA; 1984. SAE 841663.
Otte D, Haasper C. Characteristics on fractures of tibia and fibula in car impacts to pedestrians and bicyclists – influences of car bumper height and shape. *Ann Adv Automot Med*. 2007;51:63–79.
Park DK, Jang CD. Optimum suv bumper system design considering pedestrian performance. *Int J Automot Tech*. 2010;11(6):819–824.
Pehrs DMG. Study of vehicle-to-pedestrian interactions with FEM – evaluation of upper leg test methods using a human body mode. Master of Science Thesis in Medical Engineering A, School of Technology and Health, 2013.
Schuster P, Staines B. *Determination of bumper styling and engineering parameters to reduce pedestrian leg injuries*. Society of Automotive Engineers, Warrendale, PA; 1998. SAE 980361.
Schuster P. *Current trends in bumper design for pedestrian impact*. Society of Automotive Engineers, Warrendale, PA; 2006. SAE 2006-01-0464.
Yang J. Effects of vehicle front design parameters on pedestrian head-brain injury protection. Paper presented at: 18th International Technical Conference on the Enhanced Safety of Vehicles (ESV); May 19–22, 2003; Nagoya, Japan.
Yasuki T. Mechanism analysis of pedestrian knee-bending angle by sedan-type vehicle using human FE model. *Int. J. Crashworthiness*. 2007;12(4):329–339.
Yasuki T. Mechanism analysis of pedestrian knee-bending angle by SUV type vehicles using human FE model. *Int. J. Crashworthiness*. 2007;12(6):645–651.
Yasuki, T. An analysis of lower leg impactor behavior by physics model. *J Biomech Sci Eng*. 2008;3(2):151–160.
Yoshida S, Matsuhashi T, Matsuoka Y. Simulation of car-pedestrian accident for evaluate car structure. Paper presented at: 16th International Technical Conference on the Enhanced Safety of Vehicles (ESV); May 31–June 4, 1998; Windsor, Canada.
Zanetti EM, Franceschini G, Audenino AL. Lower leg injury in relation to vehicle front end. Traffic Inj Prev. 2014;15(4):395–401.
Zhang G, Cao L, Hu J, Yang KH. A field data analysis of risk factors affecting the injury risks in vehicle-to-pedestrian crashes. *Ann Adv Automot Med*. 2008;52:199–214.

APPENDIX

Literature Review

The influence of the vehicle front-end structures on the pedestrian kinematics and the pedestrian injuries were studied in many works in the past. The present literature review focuses the attention on the works related to the design of the vehicle front-end and on the injuries to the pedestrian lower limb. Considering only those studies

that were carried out with numerical tools, they took into analysis different aspects of the problem. Some works investigated the influence of the shape and the geometry of the bumper (Niederer and Schlumpf 1984; Yang 2003; Yoshida et al. 1998; Ishikawa et al. 1991; Matsui 2005; Dunmore et al. 2006; Schuster and Staines 1998; Lee et al. 2014; Liu et al. 2011; lshikawa et al. 1992). Many of these works put particular attention to the vertical position of the bumper (Ishikawa et al. 1991; Matsui 2005; Dunmore et al. 2006; lshikawa et al. 1992; Abvabi et al. 2010; Huang et al. 2011). In other works (Abvabi et al. 2010b; Huang et al. 2011), the stiffness of the bumper and more in general of the front-end structure of the vehicle was investigated. Some studies analyzed together the geometry of the bumper and its stiffness (Liu et al. 2002; Harris and Grew 1985; Zanetti et al. 2014). Moreover, many works (Schuster 2006; Davoodi et al. 2008; Cheon 1995; Moon 2012; Jiang and Yang 2012; Liu et al. 2011; Park and Jang 2010; Nagasaka 2003) deal with the investigation of innovative solutions for the front-end structures. These innovative solutions were aimed to the reduction of the injuries on the lower limb of the pedestrians. In all these previous works, the impacts with the front-end structure of the vehicle were simulated using the lower legforms developed for the execution of the experimental tests illustrated above. The numerical analysis were carried out with human leg models only in few cases (Pehrs 2013; Yasuki 2007; Yasuki 2007b; Yasuki 2008). In these last works, the authors mainly investigated the influence of the stiffness of the front-end structure.FE Models

The GCMs were numerical models not of real cars from the market but of *realistic* models of vehicles representative of the best-in-class types currently available. The idea was to give the researchers involved in safety, publicly available models to play with to develop new safety devices and strategies without the restrictions and limitations of real vehicle models. To this aim, the GCMS were *mildly* validated against the results in terms of performance of similar vehicles of the same class: *strict* validation was not possible since those GCM vehicles are not existing but, with the previous principle in mind, those models were considered useful for studies as the current research.

The GCM4 vehicle was used in this work. It is the model of an MPV based on the geometry and features of the Dodge Caravan and of the Renault Espace. The GCM4 includes the whole chassis, the wheels and the body of the vehicle with the engine. The initial model was modified to make it more similar to the best in class models according to the EuroNCAP tests. Therefore, the vehicle model includes the nowadays usual two load lines, upper and lower, as shown in Figures 2 and A1. The upper and stronger line has a supporting transverse beam made of metal and an energy absorbing element (absorber) made of plastic. The lower load line consists of a simpler plastic absorber. The GCM model was validated testing it in various conditions and comparing the obtained numerical results with the widest number of experimental tests available from external independent sources, for that type of vehicles. In this work, the GCM4 was cut with a plane perpendicular to the longitudinal axis of the vehicle at the front part of the windshield. The mass of the rear part of the cut vehicle was applied to this section by means of a rigid body. Constraints in vertical and transversal direction were also applied to this section. In this way, the vehicle model had only the longitudinal displacement as free degree of freedom.

The geometry of the LLMS was derived from magnetic resonance imaging measurements collected on a cadaver subject close to 50th percentile man. The lower limb model was made using shell, bricks and springs elements. The material properties for this model were obtained from literature. The lower limb model was validated comparing its behavior to a series of experimental tests. These tests varying from isolated tests on single parts (tissues, ligaments, bones etc.) to the whole limb impacts. As discussed by Mo, Arnoux, Cesari and Masson (2012), the kinematic behavior of the dummy model made up of these two different parts (Hybrid III model and

LLMS model) is in good correlations with the experimental results of impact test between pedestrian and vehicle, carried out in full scale conditions with post mortem human subjects (PMHS) (Masson et al. 2007).
All the simulations were performed using the explicit dynamic FEM solver RADIOSS v12 (Altair Engineering Inc., Troy, USA). No element deletions were activated in both the car model and the pedestrian model during the simulations. However, this aspect should not affect the response of the model, as demonstrated in the validation phase of the two numerical models.

Measured Biomechanical Parameters

The sections where the bending moment on the tibia was measured are shown in Figure A3.
The spring elements used to measure the ligament strains had low stiffness. These springs were attached to the elements used to model the ligaments. The springs were positioned along the middle line of the ligaments that is the main axis of the ligament fiber (Figure A4). The strain of a single ligament was evaluated as the ratio between the strain of the spring elements along their axis and their initial length (Mo, Arnoux, Cesari and Masson 2012; Mo, Arnoux, Jure and Masson 2012; Mo, Arnoux, Zahidi and Masson 2013; Mo, Masson, Cesari and Arnoux 2013; Mo et al. 2015). The ligament was considered failed when the value of the engineering strain of the entire ligament exceeded its defined strain threshold. On one hand, using this method, the LLMS model showed accurate ability to provide good assessments of the injuries of the knee ligament under complex loading conditions (Mo et al. 2014; Arnoux et al. 2005; Bose et al. 2007). On the other hand, the LLMS model could be improved implementing a ligament failure based on the strains of the shell and solid elements used to model the ligaments. However, a ligament failure based on elements deletion should be very sensitive to the element dimension. Considering a global model of lower limb used for safety research, the mesh size used for the modelling of the ligaments is not small enough. This is mainly due to considerations about the time step and the stability of the model. Consequently, a direct implementation of the element failure in the model could overestimate the ligaments failures. This is because the crack size is determined by the element size. From a physical point of view, this means that a small laxity could be translated to a total fracture in the model due to the relatively large size of the elements. The use of the global strain of the entire ligament, in the evaluation of the failure, would avoid this problem. A further improvement on the model could be represented by the use of the extended finite element method (XFEM). This method was introduced by Belytschko and Black (1999) and it was more recently implemented in the commercial FE codes. This method allows to reduce the mesh dependency when the crack initiation and propagation is simulated (Mo et al. 2014).

RESULTS

Lower Limb Kinematics

The influence of the studied parameters on the lower limb kinematics is summarized in Figures A6 and A7 for the reference configuration, $Y = 0$ and for the leg position $Y = -125$ mm respectively.
The figures depict the leg kinematics as the lines of the axes of the tibia and femur extracted, at some equally spaced times, from the displacements of selected nodes used as kinematic landmarks (Figure A5). Due to the typical time scale of the phenomenon, it was chosen to get the kinematics at four times from 10 to 40 ms with an interval of 10 ms.

Knee Ligaments

Figures A8 and A9 report the influence of the parameters considered in the work in terms of knee ligament strains for the Medium Collateral Ligament (MCL), the Posterior Cruciate Ligament (PCL) the Anterior Cruciate Ligament (ACL) and the Lateral Collateral Ligament (LCL). The Figure A8 is related to the reference transverse offset $Y = 0$ whereas the Figure A9 refers to the leg position $Y = -125$ mm. In these figures, the measured strains are plotted as a function of time from 5 to 15 ms. The maximum values of the ordinate axis of the charts of the ligament strains were fixed to the threshold values of the ligament failure discussed in the Methods section.

Bending

Figures A10 and A11 show the results from the parametric analysis in terms of: tibia bending moment as a function of the position along the tibia axis from the tibia plateau; maximum tibia bending moment as a function of the simulation time; average bending moment as a function of time. Figure A10 refers to the reference position $Y = 0$ whereas the Figure A11 refers to the leg position $Y = -125$ mm.

LIMITATIONS AND FUTURE DEVELOPMENTS

In this work, a DOE analysis was done considering individually each parameter. In future work a deeper study can be carried out, doing a more complex DOE investigating the correlation between the different parameters.
A main limitation of the current study relates to the limited range of variation of the various parameters and considering a single value of the speed: as clearly shown by Matsui (2005) increasing the impact speed can lead to ligament failures not occurring at lower speed. In the current study, the impact speed was kept constant at the typical value of the pedestrian safety tests, which, in turns, was fixed as the most significant of typical real accident scenarios. Moreover, the obtained results give hints about the failure of ligaments and tibia but cannot be directly related to injury levels, and therefore directly compared with field data. Another problem in comparing with real accidents observations lies in the fact that generally only the outer envelope of the vehicle is considered whereas the internal details, and in particular the typical current construction with the two load lines, are not kept into account.

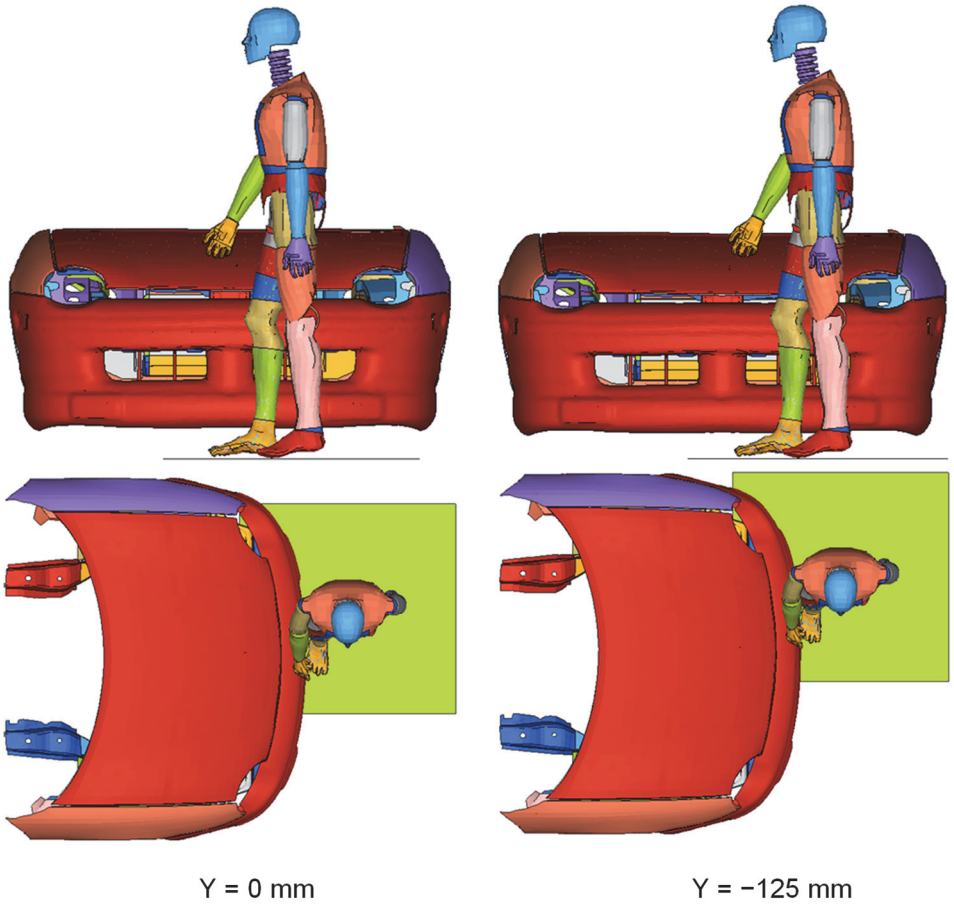


Fig. 1. Front and top view of the considered configurations of the vehicle-pedestrian impacts. Two different positions in terms of transverse offset Y for the Hybrid III dummy with the biofidelic LLMS model were considered: on the left hand side the reference position ($Y = 0$, leg in the middle of the bumper), on the right hand side the displaced position ($Y = -125$ mm).

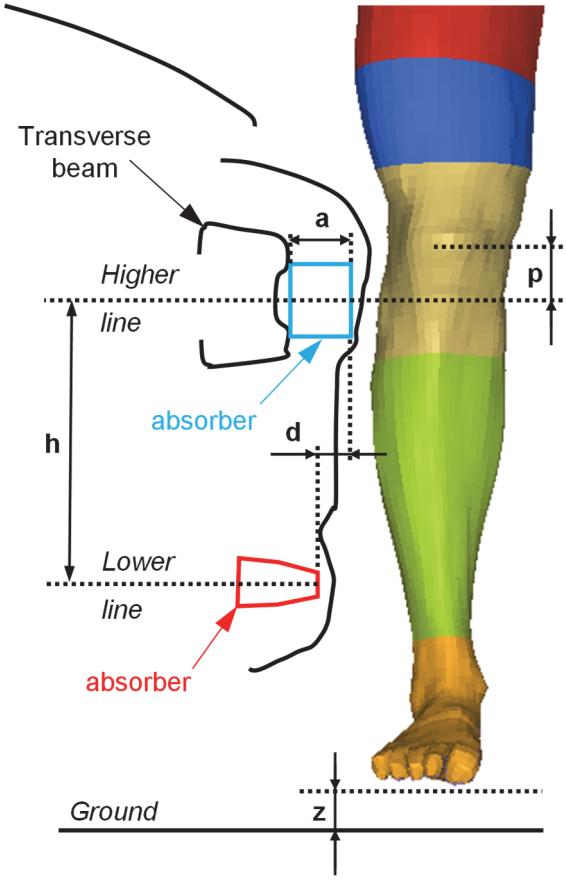


Fig. 2. Side view of the passenger vehicle-pedestrian interface: geometric details are put in evidence.

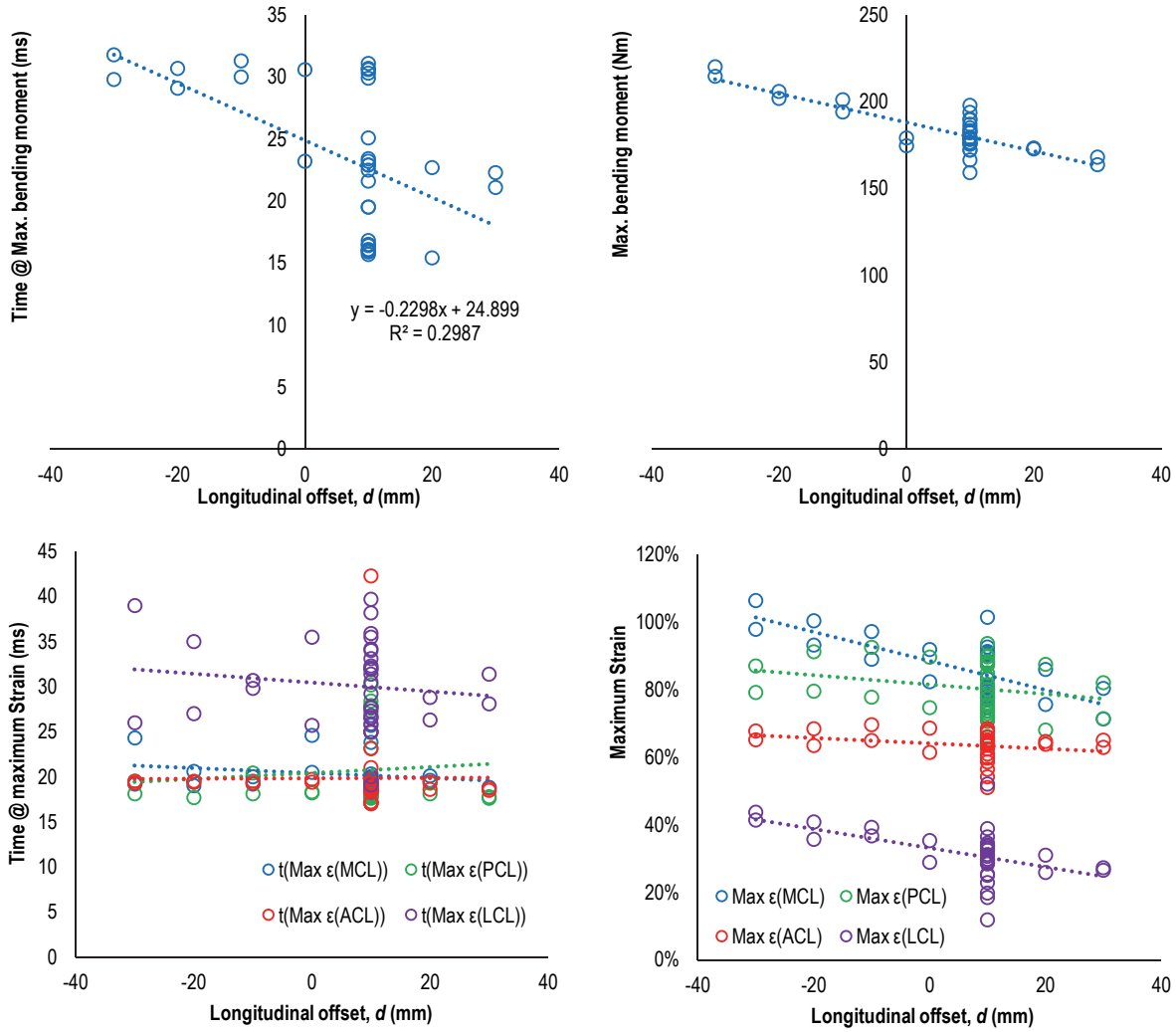


Fig. 3. Influence of the longitudinal offset *d* on the outputs in terms of time corresponding to its maximum values (on the left hand side) and in terms of maximum values (on the right hand side): above, considering the maximum bending moment; below, considering the maximum ligament strains

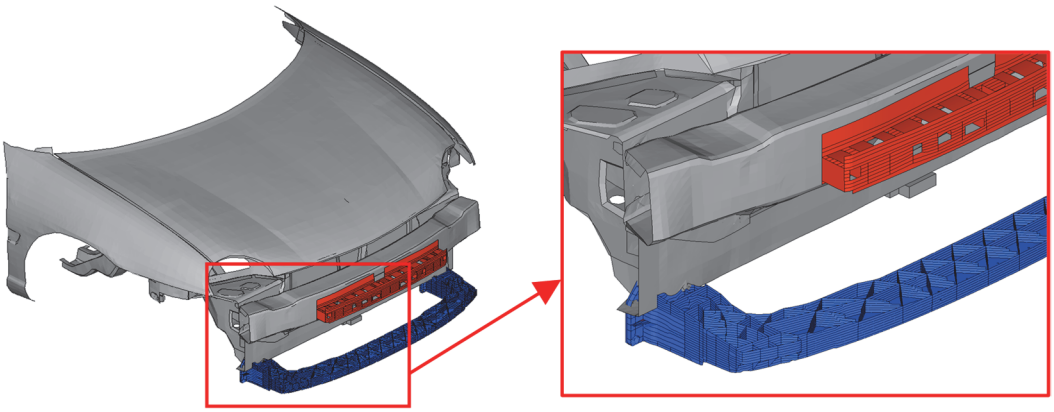


Fig. A1. Front view of the vehicle model without the bumper fascia. In evidence the two plastic absorbers: the higher one in red and the lower one in blue.

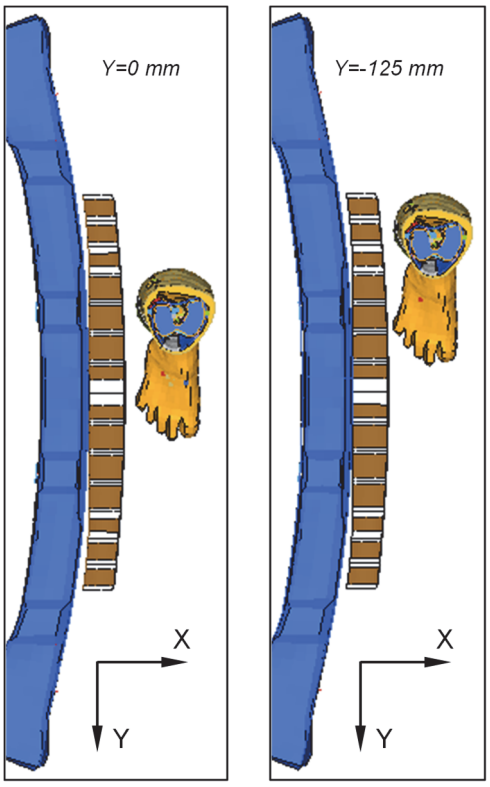


Fig. A2. Top view of a horizontal section of the leg and vehicle front-end showing the variation in the transverse Y position: left, the leg is in the reference position ($Y = 0$) complete facing the absorber; right, the leg is in an offset position of $Y = -125$ mm, facing the edge end of the absorber (in blue the bumper beam, in brown the absorber).



Fig. A3. Lower part of the LLMS model: in blue the sections where the bending moment on the tibia was measured.

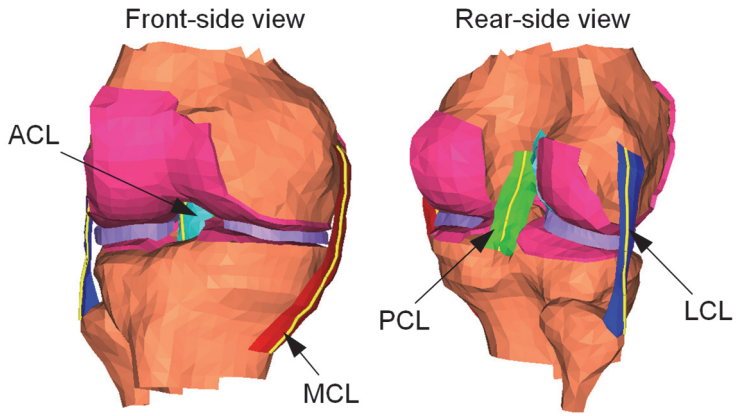


Fig. A4. Detail of the LLMS model in the knee region. The knee ligaments are put in evidence with different colors: ACL in light blue, PCL in green, MCL in red and LCL in blue. The spring elements used to measure the knee ligament strains are shown in yellow.

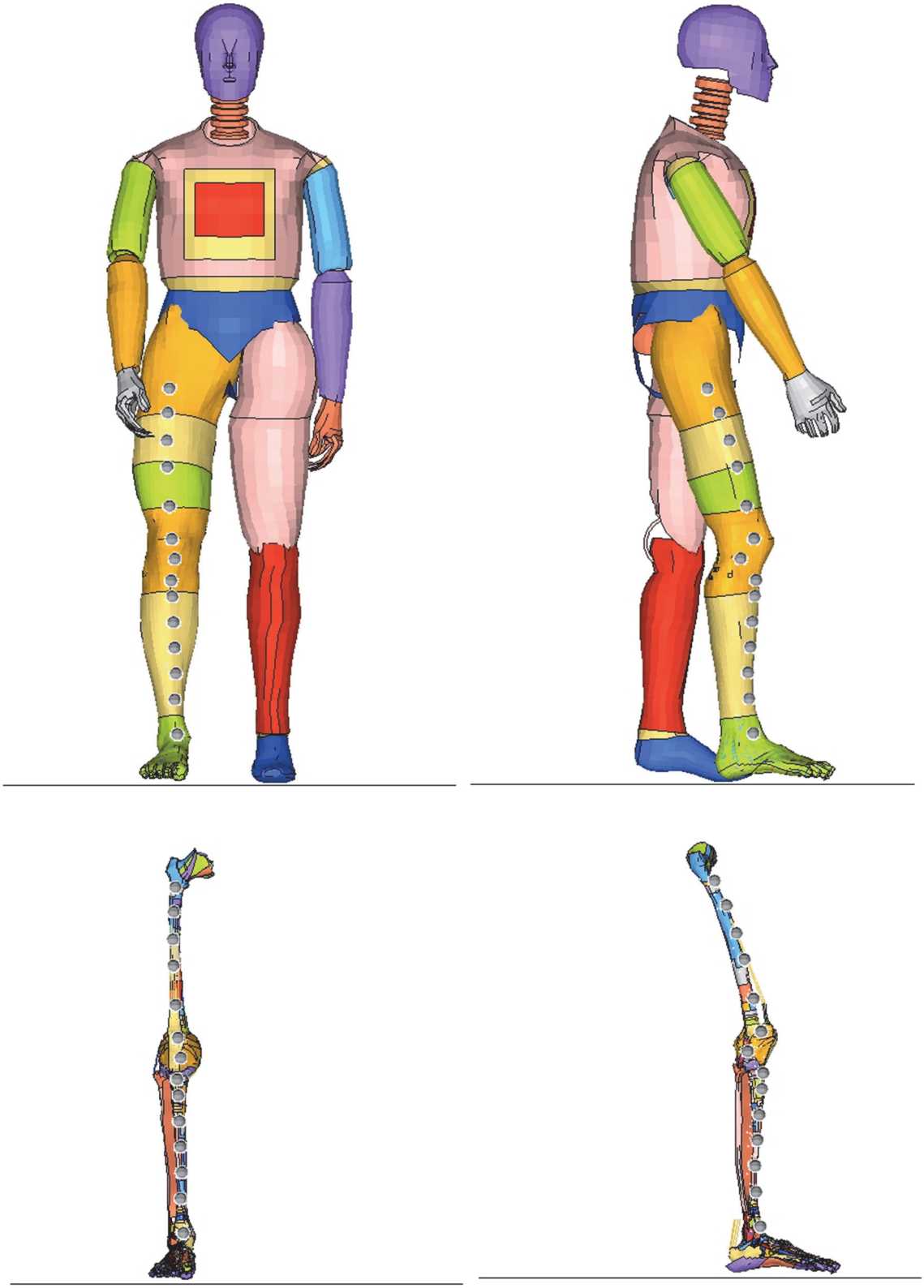
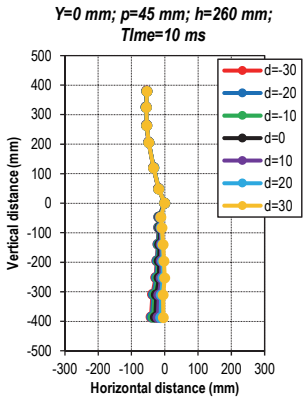
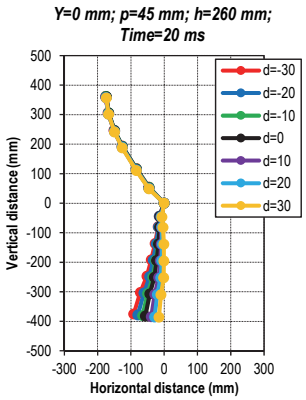
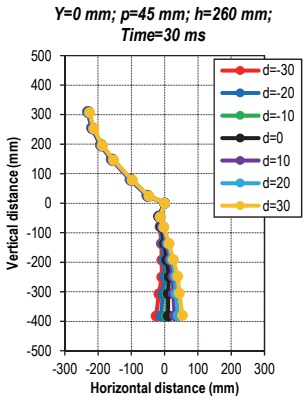
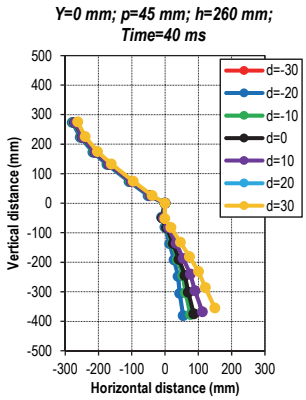


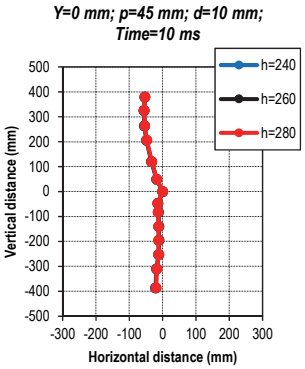
Fig. A5. The anatomical location of the kinematic landmarks used to study the leg deformation.

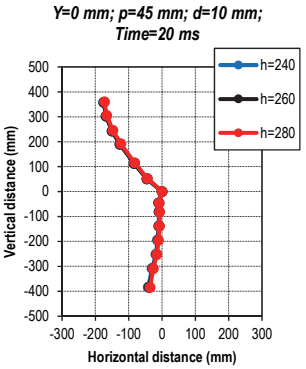

Y=0 mm; p=45 mm; h=260 mm;
TIme=10 ms
Vertical distance (mm)
Horizontal distance (mm)
d=-30
d=-20
d=-10
d=0
d=10
d=20
d=30

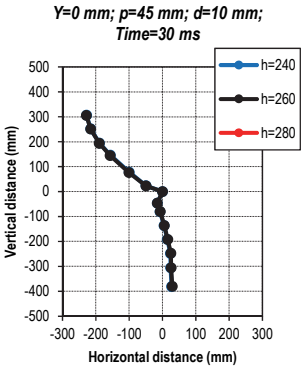

Y=0 mm; p=45 mm; h=260 mm;
Time=20 ms
Vertical distance (mm)
Horizontal distance (mm)
d=-30
d=-20
d=-10
d=0
d=10
d=20
d=30

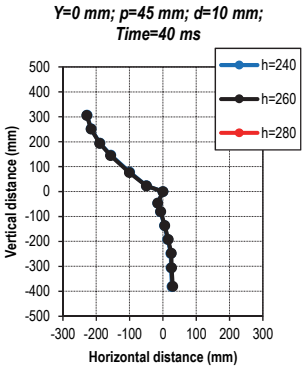

Y=0 mm; p=45 mm; h=260 mm;
Time=30 ms
Vertical distance (mm)
Horizontal distance (mm)
d=-30
d=-20
d=-10
d=0
d=10
d=20
d=30

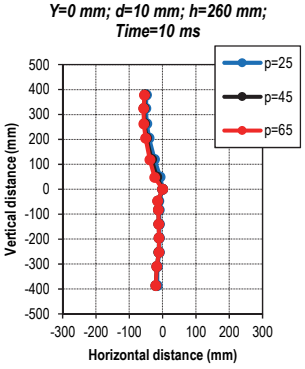

Y=0 mm; p=45 mm; h=260 mm;
Time=40 ms
Vertical distance (mm)
Horizontal distance (mm)
d=-30
d=-20
d=-10
d=0
d=10
d=20
d=30

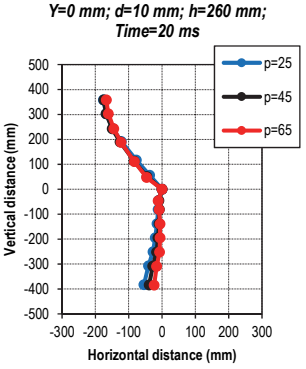

Y=0 mm; p=45 mm; d=10 mm;
Time=10 ms
Vertical distance (mm)
Horizontal distance (mm)
h=240
h=260
h=280

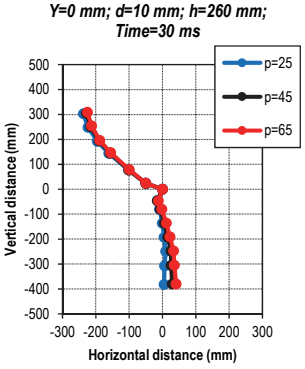

Y=0 mm; p=45 mm; d=10 mm;
Time=20 ms
Vertical distance (mm)
Horizontal distance (mm)
h=240
h=260
h=280

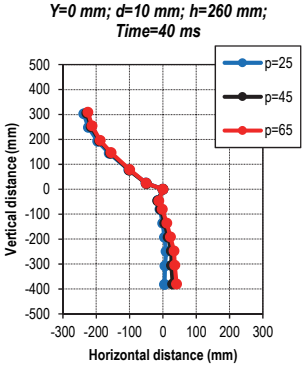

Y=0 mm; p=45 mm; d=10 mm;
Time=30 ms
Vertical distance (mm)
Horizontal distance (mm)
h=240
h=260
h=280

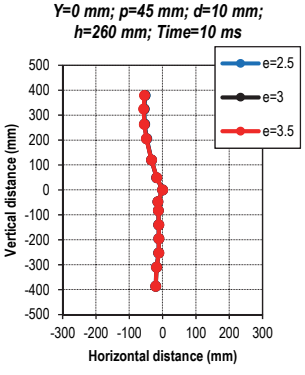

Y=0 mm; p=45 mm; d=10 mm;
Time=40 ms
Vertical distance (mm)
Horizontal distance (mm)
h=240
h=260
h=280

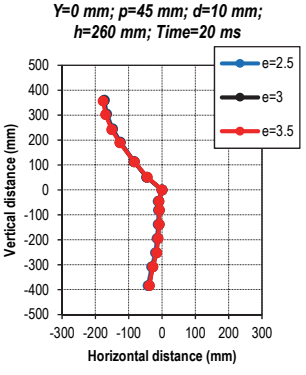

Y=0 mm; d=10 mm; h=260 mm;
Time=10 ms
Vertical distance (mm)
Horizontal distance (mm)
p=25
p=45
p=65

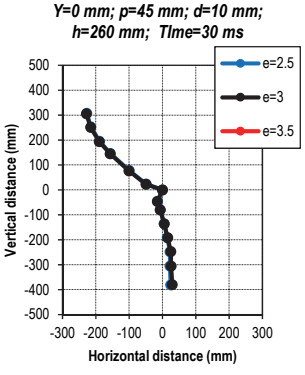

Y=0 mm; d=10 mm; h=260 mm;
Time=20 ms
Vertical distance (mm)
Horizontal distance (mm)
p=25
p=45
p=65

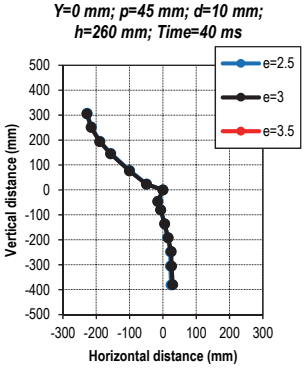

Y=0 mm; d=10 mm; h=260 mm;
Time=30 ms
Vertical distance (mm)
Horizontal distance (mm)
p=25
p=45
p=65

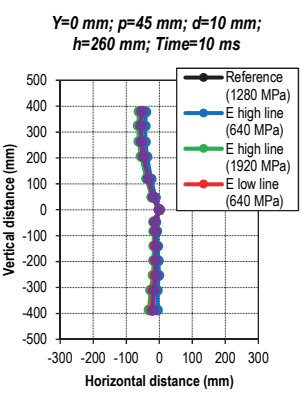

Y=0 mm; d=10 mm; h=260 mm;
Time=40 ms
Vertical distance (mm)
Horizontal distance (mm)
p=25
p=45
p=65

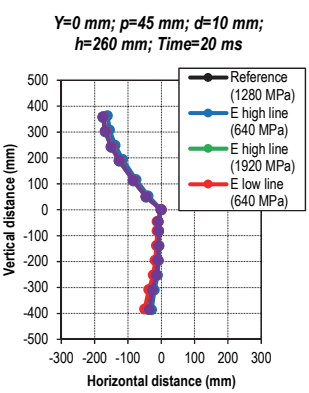

Y=0 mm; p=45 mm; d=10 mm;
h=260 mm; Time=10 ms
Vertical distance (mm)
Horizontal distance (mm)
e=2.5
e=3
e=3.5

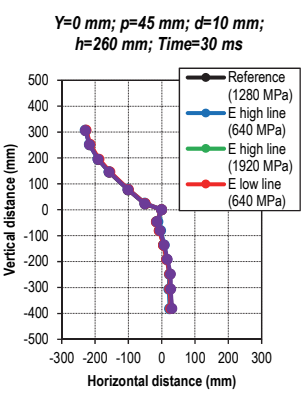

Y=0 mm; p=45 mm; d=10 mm;
h=260 mm; Time=20 ms
Vertical distance (mm)
Horizontal distance (mm)
e=2.5
e=3
e=3.5


Y=0 mm; p=45 mm; d=10 mm;
h=260 mm; TIme=30 ms
Vertical distance (mm)
Horizontal distance (mm)
e=2.5
e=3
e=3.5


Y=0 mm; p=45 mm; d=10 mm;
h=260 mm; Time=40 ms
Vertical distance (mm)
Horizontal distance (mm)
e=2.5
e=3
e=3.5


Y=0 mm; p=45 mm; d=10 mm;
h=260 mm; Time=10 ms
Vertical distance (mm)
Horizontal distance (mm)
Reference (1280 MPa)
E high line (640 MPa)
E high line (1920 MPa)
E low line (640 MPa)


Y=0 mm; p=45 mm; d=10 mm;
h=260 mm; Time=20 ms
Vertical distance (mm)
Horizontal distance (mm)
Reference (1280 MPa)
E high line (640 MPa)
E high line (1920 MPa)
E low line (640 MPa)


Y=0 mm; p=45 mm; d=10 mm;
h=260 mm; Time=30 ms
Vertical distance (mm)
Horizontal distance (mm)
Reference (1280 MPa)
E high line (640 MPa)
E high line (1920 MPa)
E low line (640 MPa)

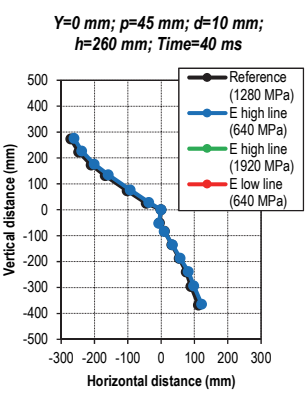
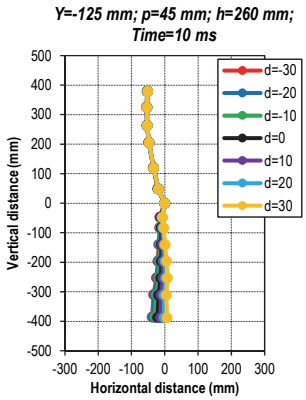
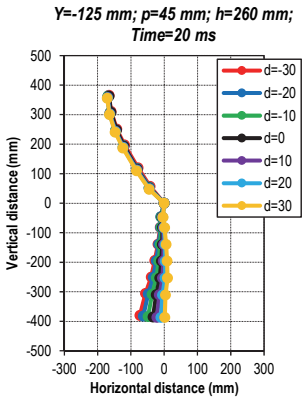
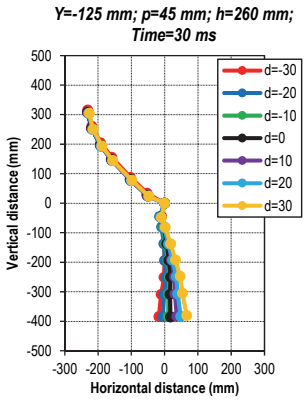
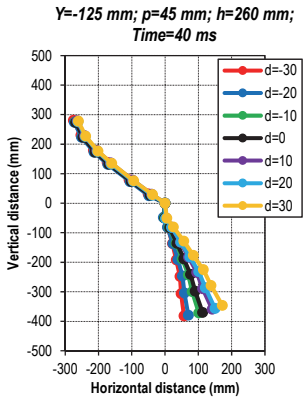

Y=0 mm; p=45 mm; d=10 mm;
h=260 mm; Time=40 ms
Vertical distance (mm)
Horizontal distance (mm)
Reference (1280 MPa)
E high line (640 MPa)
E high line (1920 MPa)
E low line (640 MPa)

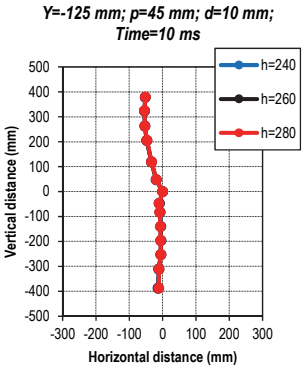
Fig. A6. Influence of the all considered parameters on the lower extremity kinematics during vehicle–pedestrian collisions, for the leg position $Y = 0$ ('vertical distance' indicates the relative vertical distance of all selected points to the joint center in the coronal plane; 'horizontal distance' indicates the horizontal relative distance of all selected points to the joint center in the coronal plane). Four different instant time (10, 20, 30, 40 ms) during the collision were considered, they are shown from the left to the right. Each line shows the influence of a different parameter.

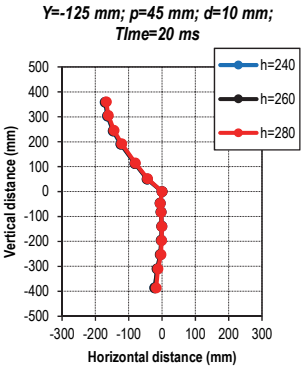

Y=-125 mm; p=45 mm; h=260 mm; Time=10 ms
d=-30
d=-20
d=-10
d=0
d=10
d=20
d=30
Vertical distance (mm)
Horizontal distance (mm)

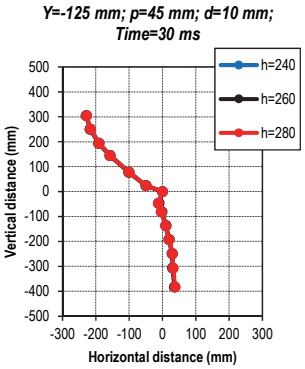

Y=-125 mm; p=45 mm; h=260 mm; Time=20 ms
d=-30
d=-20
d=-10
d=0
d=10
d=20
d=30
Vertical distance (mm)
Horizontal distance (mm)

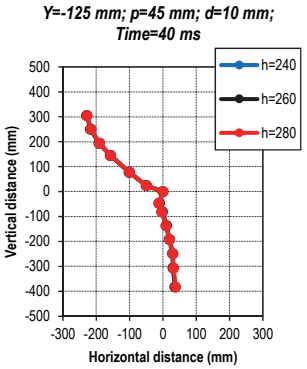

Y=-125 mm; p=45 mm; h=260 mm; Time=30 ms
d=-30
d=-20
d=-10
d=0
d=10
d=20
d=30
Vertical distance (mm)
Horizontal distance (mm)

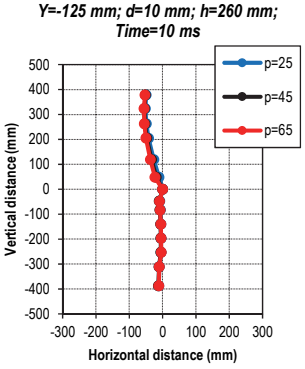

Y=-125 mm; p=45 mm; h=260 mm; Time=40 ms
d=-30
d=-20
d=-10
d=0
d=10
d=20
d=30
Vertical distance (mm)
Horizontal distance (mm)

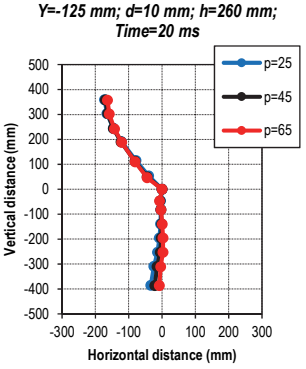

Y=-125 mm; p=45 mm; d=10 mm; Time=10 ms
h=240
h=260
h=280
Vertical distance (mm)
Horizontal distance (mm)

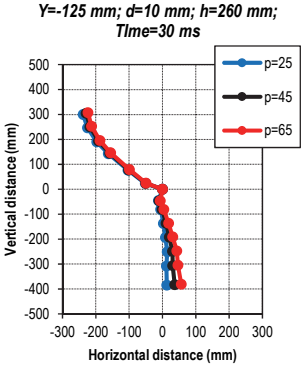

Y=-125 mm; p=45 mm; d=10 mm; TIme=20 ms
h=240
h=260
h=280
Vertical distance (mm)
Horizontal distance (mm)

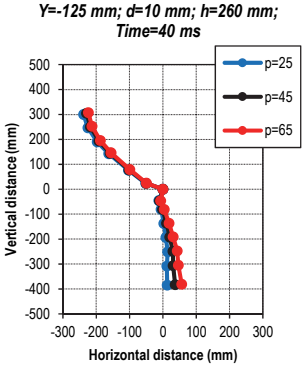

Y=-125 mm; p=45 mm; d=10 mm; Time=30 ms
h=240
h=260
h=280
Vertical distance (mm)
Horizontal distance (mm)

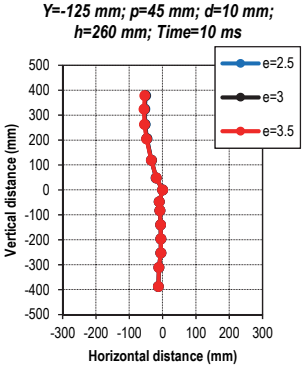

Y=-125 mm; p=45 mm; d=10 mm; Time=40 ms
h=240
h=260
h=280
Vertical distance (mm)
Horizontal distance (mm)

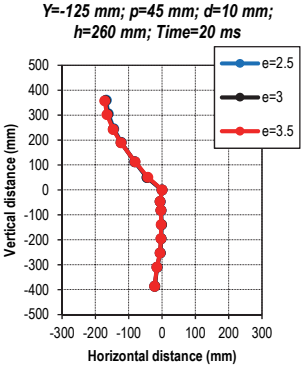

Y=-125 mm; d=10 mm; h=260 mm; Time=10 ms
p=25
p=45
p=65
Vertical distance (mm)
Horizontal distance (mm)

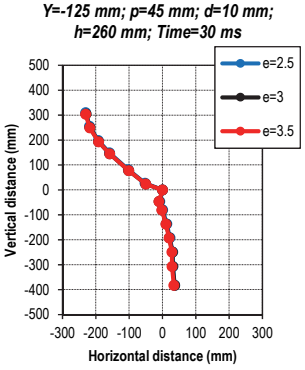

Y=-125 mm; d=10 mm; h=260 mm; Time=20 ms
p=25
p=45
p=65
Vertical distance (mm)
Horizontal distance (mm)

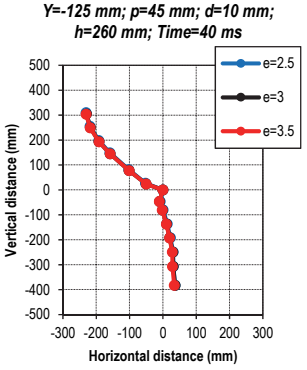

Y=-125 mm; d=10 mm; h=260 mm; TIme=30 ms
p=25
p=45
p=65
Vertical distance (mm)
Horizontal distance (mm)

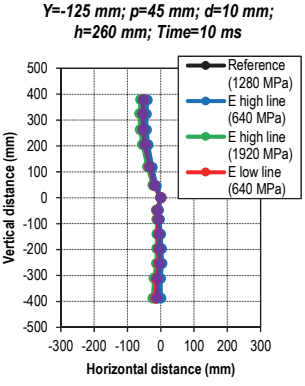

Y=-125 mm; d=10 mm; h=260 mm; Time=40 ms
p=25
p=45
p=65
Vertical distance (mm)
Horizontal distance (mm)

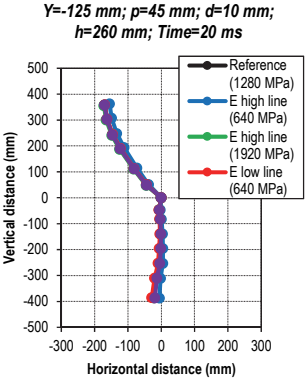

Y=-125 mm; p=45 mm; d=10 mm; h=260 mm; Time=10 ms
e=2.5
e=3
e=3.5
Vertical distance (mm)
Horizontal distance (mm)

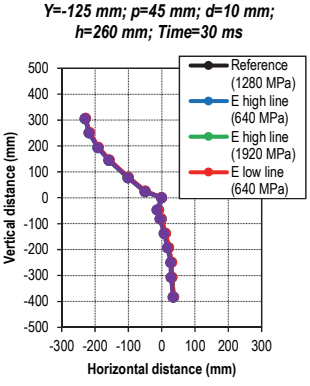

Y=-125 mm; p=45 mm; d=10 mm; h=260 mm; Time=20 ms
e=2.5
e=3
e=3.5
Vertical distance (mm)
Horizontal distance (mm)


Y=-125 mm; p=45 mm; d=10 mm; h=260 mm; Time=30 ms
e=2.5
e=3
e=3.5
Vertical distance (mm)
Horizontal distance (mm)


Y=-125 mm; p=45 mm; d=10 mm; h=260 mm; Time=40 ms
e=2.5
e=3
e=3.5
Vertical distance (mm)
Horizontal distance (mm)


Y=-125 mm; p=45 mm; d=10 mm; h=260 mm; Time=10 ms
Reference (1280 MPa)
E high line (640 MPa)
E high line (1920 MPa)
E low line (640 MPa)
Vertical distance (mm)
Horizontal distance (mm)


Y=-125 mm; p=45 mm; d=10 mm; h=260 mm; Time=20 ms
Reference (1280 MPa)
E high line (640 MPa)
E high line (1920 MPa)
E low line (640 MPa)
Vertical distance (mm)
Horizontal distance (mm)


Y=-125 mm; p=45 mm; d=10 mm; h=260 mm; Time=30 ms
Reference (1280 MPa)
E high line (640 MPa)
E high line (1920 MPa)
E low line (640 MPa)
Vertical distance (mm)
Horizontal distance (mm)

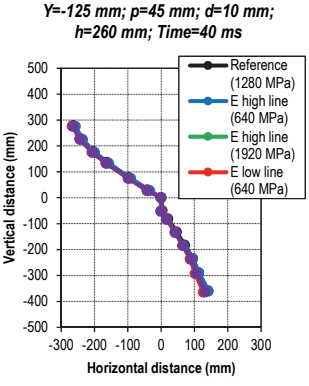

Y=-125 mm; p=45 mm; d=10 mm; h=260 mm; Time=40 ms
Reference (1280 MPa)
E high line (640 MPa)
E high line (1920 MPa)
E low line (640 MPa)
Vertical distance (mm)
Horizontal distance (mm)

Fig. A7. Influence of the all considered parameters on the lower extremity kinematics during vehicle - pedestrian collisions, for the leg position $Y = -125$ mm ('vertical distance' indicates the relative vertical distance of all selected points to the joint center in the coronal plane; 'horizontal distance' indicates the horizontal relative distance of all selected points to the joint center in the coronal plane). Four different instant time (10, 20, 30, 40 ms) during the collision were considered, they are shown from the left to the right. Each line shows the influence of a different parameter.

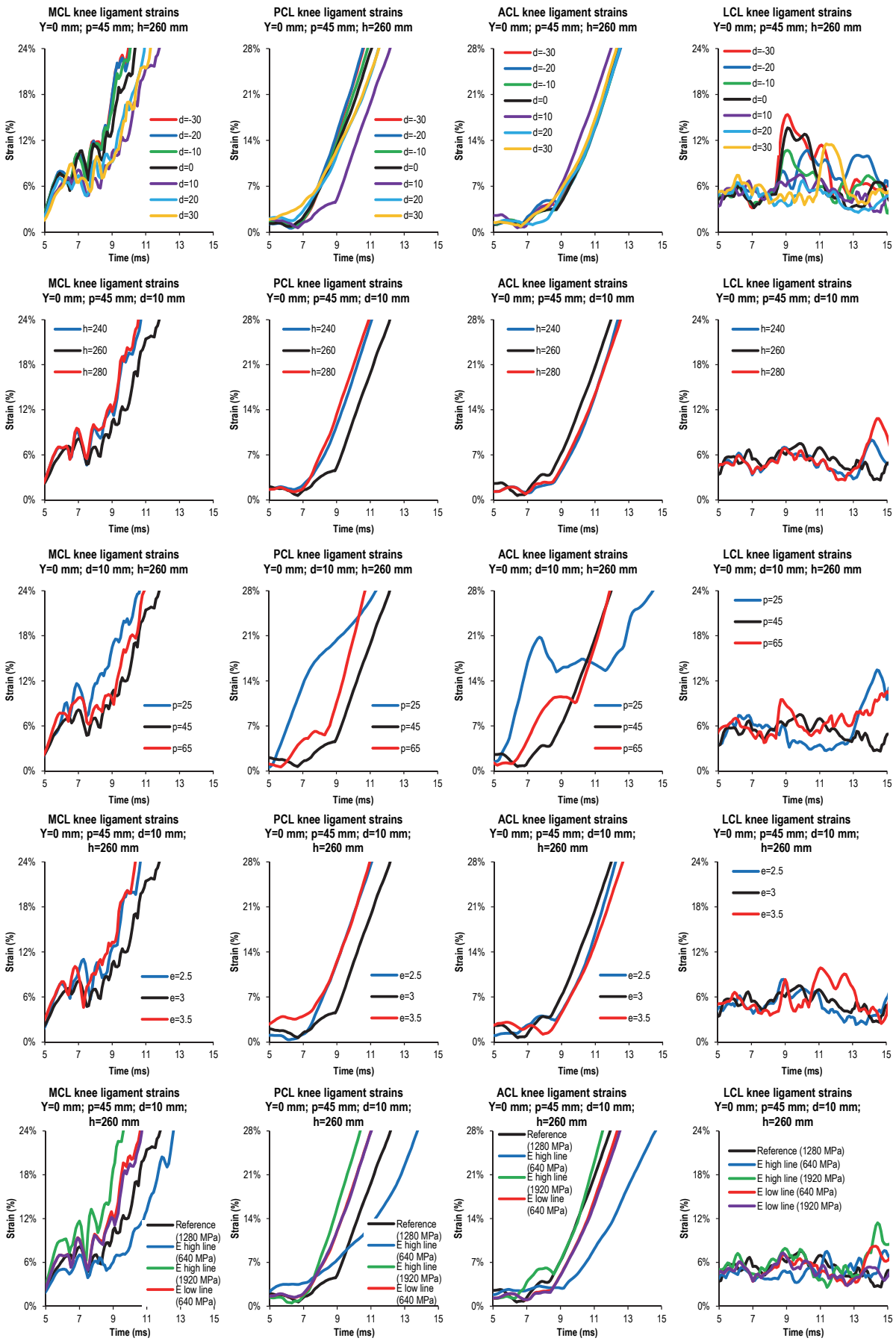

MCL knee ligament strains
Y=0 mm; p=45 mm; h=260 mm
PCL knee ligament strains
Y=0 mm; p=45 mm; h=260 mm
ACL knee ligament strains
Y=0 mm; p=45 mm; h=260 mm
LCL knee ligament strains
Y=0 mm; p=45 mm; h=260 mm
d=-30
d=-20
d=-10
d=0
d=10
d=20
d=30
MCL knee ligament strains
Y=0 mm; p=45 mm; d=10 mm
PCL knee ligament strains
Y=0 mm; p=45 mm; d=10 mm
ACL knee ligament strains
Y=0 mm; p=45 mm; d=10 mm
LCL knee ligament strains
Y=0 mm; p=45 mm; d=10 mm
h=240
h=260
h=280
MCL knee ligament strains
Y=0 mm; d=10 mm; h=260 mm
PCL knee ligament strains
Y=0 mm; d=10 mm; h=260 mm
ACL knee ligament strains
Y=0 mm; d=10 mm; h=260 mm
LCL knee ligament strains
Y=0 mm; d=10 mm; h=260 mm
p=25
p=45
p=65
MCL knee ligament strains
Y=0 mm; p=45 mm; d=10 mm;
h=260 mm
PCL knee ligament strains
Y=0 mm; p=45 mm; d=10 mm;
h=260 mm
ACL knee ligament strains
Y=0 mm; p=45 mm; d=10 mm;
h=260 mm
LCL knee ligament strains
Y=0 mm; p=45 mm; d=10 mm;
h=260 mm
e=2.5
e=3
e=3.5
MCL knee ligament strains
Y=0 mm; p=45 mm; d=10 mm;
h=260 mm
PCL knee ligament strains
Y=0 mm; p=45 mm; d=10 mm;
h=260 mm
ACL knee ligament strains
Y=0 mm; p=45 mm; d=10 mm;
h=260 mm
LCL knee ligament strains
Y=0 mm; p=45 mm; d=10 mm;
h=260 mm
Reference (1280 MPa)
E high line (640 MPa)
E high line (1920 MPa)
E low line (640 MPa)
E low line (1920 MPa)
Strain (%)
Time (ms)

Fig. A8. Influence of the various considered parameters on the ligament strains for the reference leg position $Y = 0$. Each line shows the influence of a different parameter, each column shows a different knee ligament.

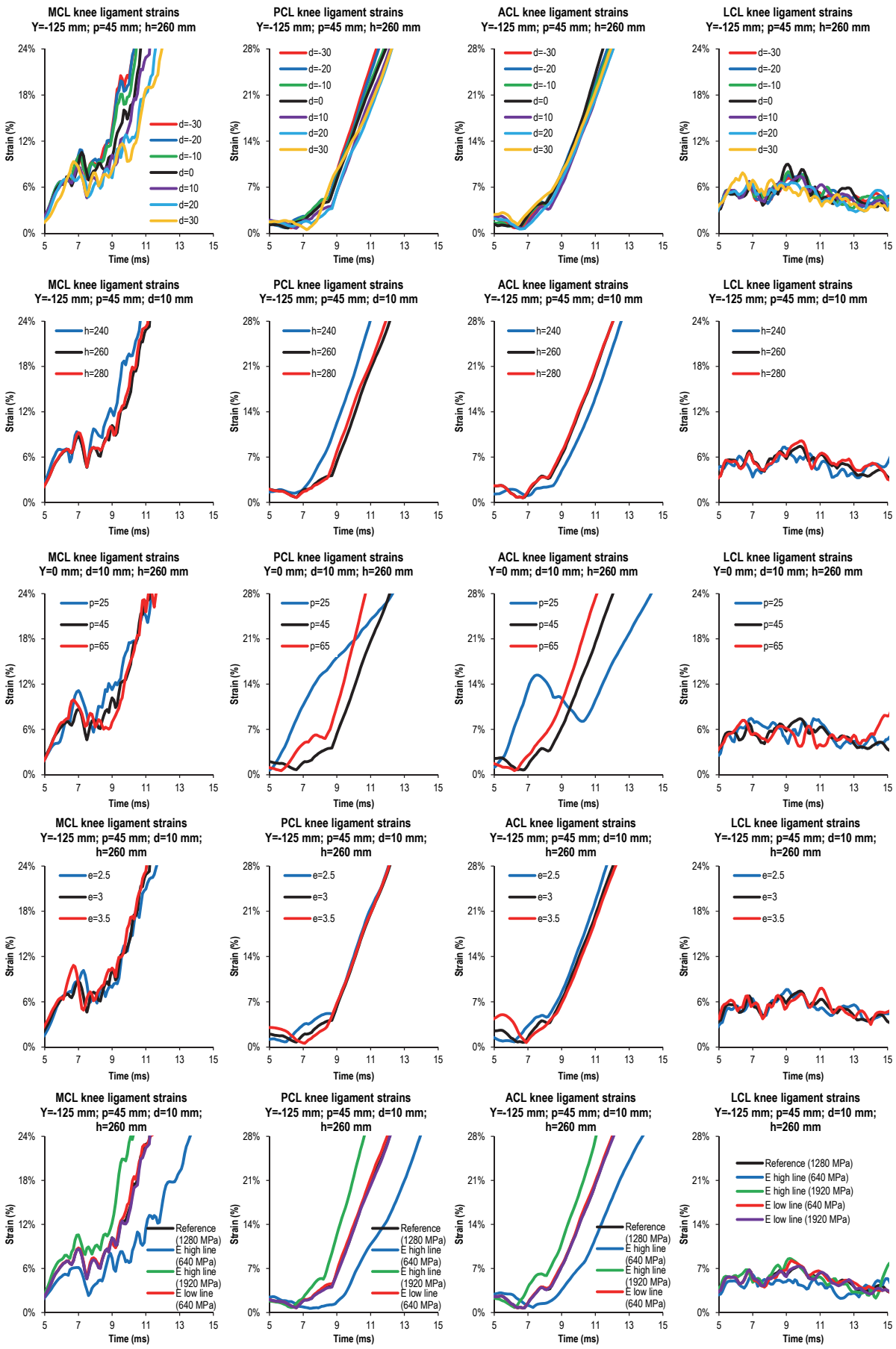
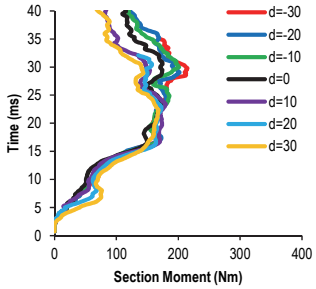
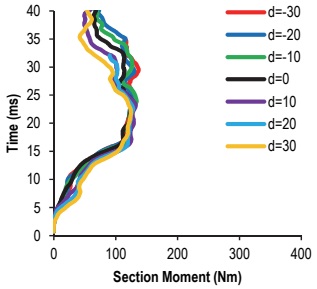

MCL knee ligament strains
Y=-125 mm; p=45 mm; h=260 mm
PCL knee ligament strains
Y=-125 mm; p=45 mm; h=260 mm
ACL knee ligament strains
Y=-125 mm; p=45 mm; h=260 mm
LCL knee ligament strains
Y=-125 mm; p=45 mm; h=260 mm
d=-30
d=-20
d=-10
d=0
d=10
d=20
d=30
MCL knee ligament strains
Y=-125 mm; p=45 mm; d=10 mm
PCL knee ligament strains
Y=-125 mm; p=45 mm; d=10 mm
ACL knee ligament strains
Y=-125 mm; p=45 mm; d=10 mm
LCL knee ligament strains
Y=-125 mm; p=45 mm; d=10 mm
h=240
h=260
h=280
MCL knee ligament strains
Y=0 mm; d=10 mm; h=260 mm
PCL knee ligament strains
Y=0 mm; d=10 mm; h=260 mm
ACL knee ligament strains
Y=0 mm; d=10 mm; h=260 mm
LCL knee ligament strains
Y=0 mm; d=10 mm; h=260 mm
p=25
p=45
p=65
MCL knee ligament strains
Y=-125 mm; p=45 mm; d=10 mm;
h=260 mm
PCL knee ligament strains
Y=-125 mm; p=45 mm; d=10 mm;
h=260 mm
ACL knee ligament strains
Y=-125 mm; p=45 mm; d=10 mm;
h=260 mm
LCL knee ligament strains
Y=-125 mm; p=45 mm; d=10 mm;
h=260 mm
e=2.5
e=3
e=3.5
MCL knee ligament strains
Y=-125 mm; p=45 mm; d=10 mm;
h=260 mm
PCL knee ligament strains
Y=-125 mm; p=45 mm; d=10 mm;
h=260 mm
ACL knee ligament strains
Y=-125 mm; p=45 mm; d=10 mm;
h=260 mm
LCL knee ligament strains
Y=-125 mm; p=45 mm; d=10 mm;
h=260 mm
Reference (1280 MPa)
E high line (640 MPa)
E high line (1920 MPa)
E low line (640 MPa)
E low line (1920 MPa)
Strain (%)
Time (ms)

Fig. A9. Influence of the various considered parameters on the ligament strains for the reference leg position $Y = -125$ mm. Each line shows the influence of a different parameter, each column shows a different knee ligament.

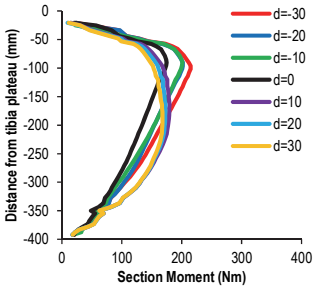
Maximum bending moment vs time
Y=0 mm; p=45 mm; h=260 mm



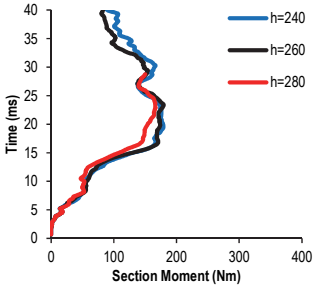
Medium bending moment vs time
Y=0 mm; p=45 mm; h=260 mm



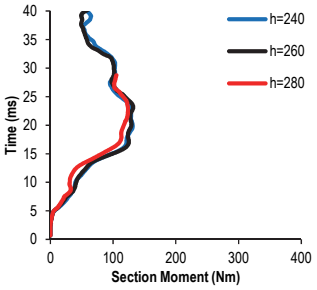
Bending moments of different positions
Y=0 mm; p=45 mm; h=260 mm



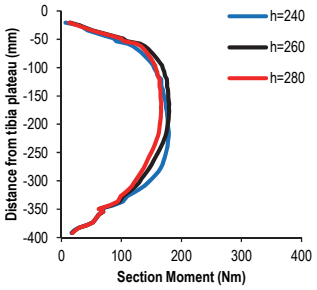
Maximum bending moment vs time
Y=0 mm; p=45 mm; d=10 mm



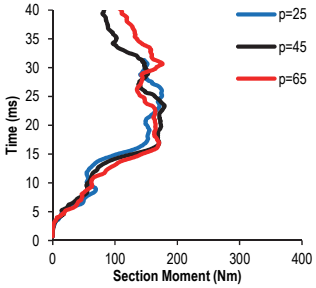
Medium bending moment vs time
Y=0 mm; p=45 mm; d=10 mm



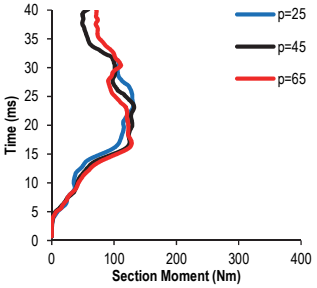
Bending moments of different positions
Y=0 mm; p=45 mm; d=10 mm



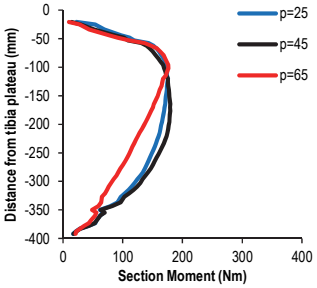
Maximum bending moment vs time
Y=0 mm; d=10 mm; h=260 mm



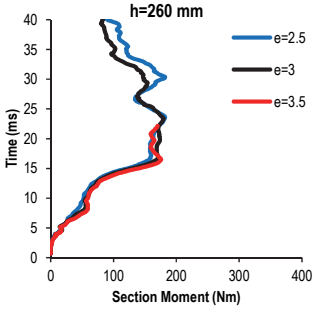
Medium bending moment vs time
Y=0 mm; d=10 mm; h=260 mm



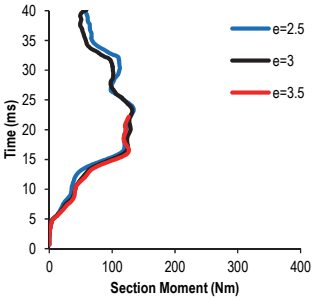
Bending moments of different positions
Y=0 mm; d=10 mm; h=260 mm



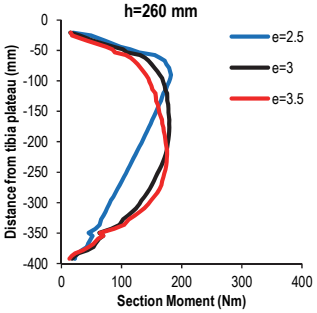
Maximum bending moment vs time
Y=0 mm; p=45 mm; d=10 mm; h=260 mm



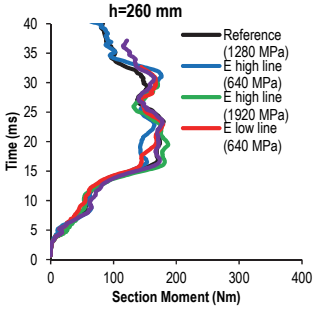
Medium bending moment vs time
Y=0 mm; p=45 mm; d=10 mm; h=260 mm



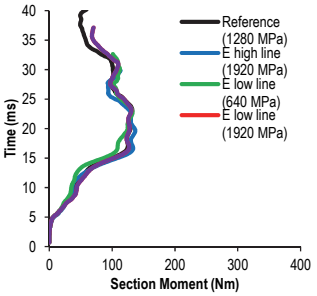
Bending moments of different positions
Y=0 mm; p=45 mm; d=10 mm; h=260 mm



Maximum bending moment vs time
Y=0 mm; p=45 mm; d=10 mm; h=260 mm



Medium bending moment vs time
Y=0 mm; p=45 mm; d=10 mm; h=260 mm



Bending moments of different positions
Y=0 mm; p=45 mm; d=10 mm; h=260 mm

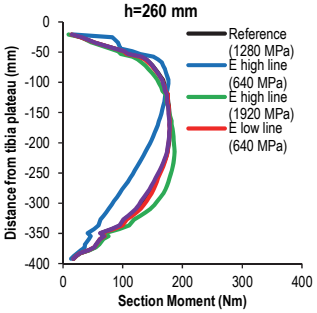
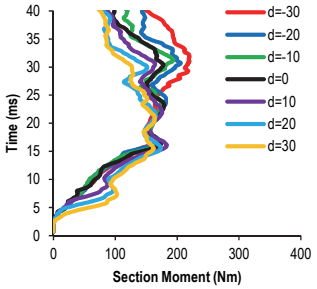
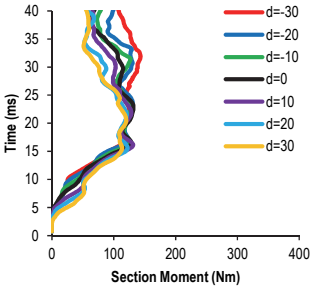


Fig. A10. Influence of the various parameters considered on the bending moment for the reference leg position $Y = 0$. From the left to the right: maximum value of the bending moment as a function of the simulation time; average value of the bending moment as a function of the simulation time; bending moment along the tibia. Each line shows the influence of a different parameter. Each line shows the influence of a different parameter.

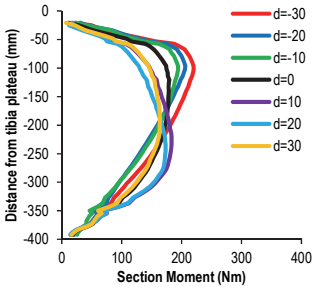
Maximum bending moment vs time
Y=-125 mm; p=45 mm; h=260 mm



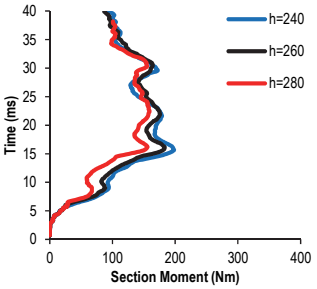
Medium bending moment vs time
Y=-125 mm; p=45 mm; h=260 mm



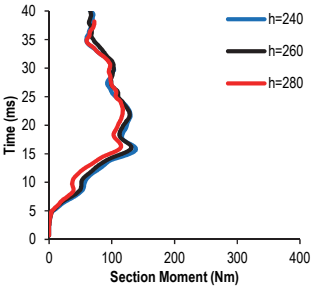
Bending moments of different positions
Y=-125 mm; p=45 mm; h=260 mm



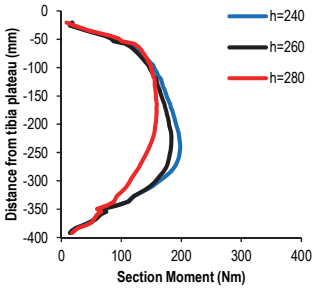
Maximum bending moment vs time
Y=-125 mm; p=45 mm; d=10 mm



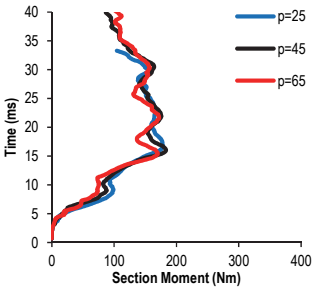
Medium bending moment vs time
Y=-125 mm; p=45 mm; d=10 mm



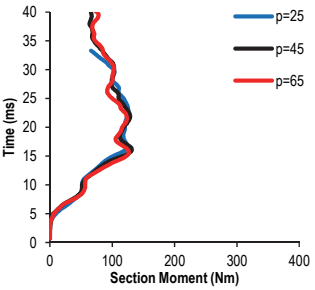
Bending moments of different positions
Y=-125 mm; p=45 mm; d=10 mm



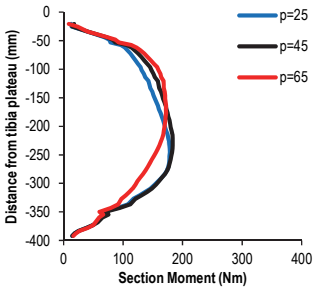
Maximum bending moment vs time
Y=-125 mm; d=10 mm; h=260 mm



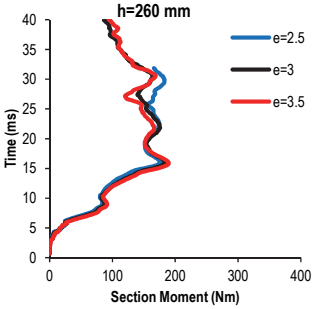
Medium bending moment vs time
Y=-125 mm; d=10 mm; h=260 mm



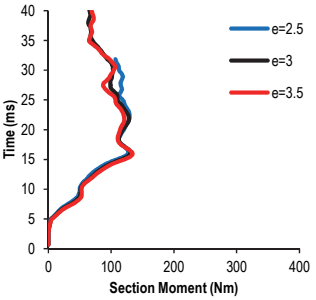
Bending moments of different positions
Y=-125 mm; d=10 mm; h=260 mm



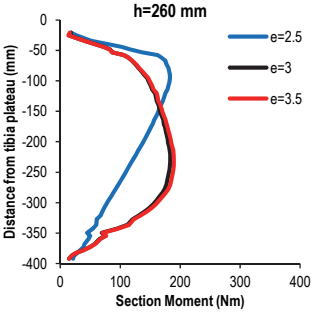
Maximum bending moment vs time
Y=-125 mm; p=45 mm; d=10 mm; h=260 mm



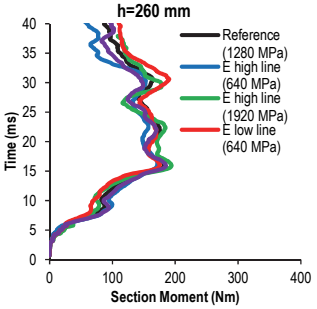
Medium bending moment vs time
Y=-125 mm; p=45 mm; d=10 mm; h=260 mm



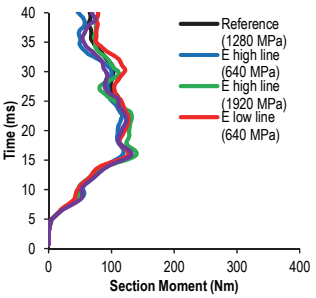
Bending moments of different positions
Y=-125 mm; p=45 mm; d=10 mm; h=260 mm



Maximum bending moment vs time
Y=-125 mm; p=45 mm; d=10 mm; h=260 mm



Medium bending moment vs time
Y=-125 mm; p=45 mm; d=10 mm; h=260 mm



Bending moments of different positions
Y=-125 mm; p=45 mm; d=10 mm; h=260 mm

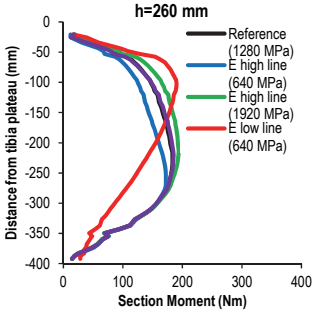


Fig. A11. Influence of the various parameters considered on the bending moment for the reference leg position $Y = -125$ mm. From the left to the right: maximum value of the bending moment as a function of the simulation time; average value of the bending moment as a function of the simulation time; bending moment along the tibia. Each line shows the influence of a different parameter. Each line shows the influence of a different parameter.

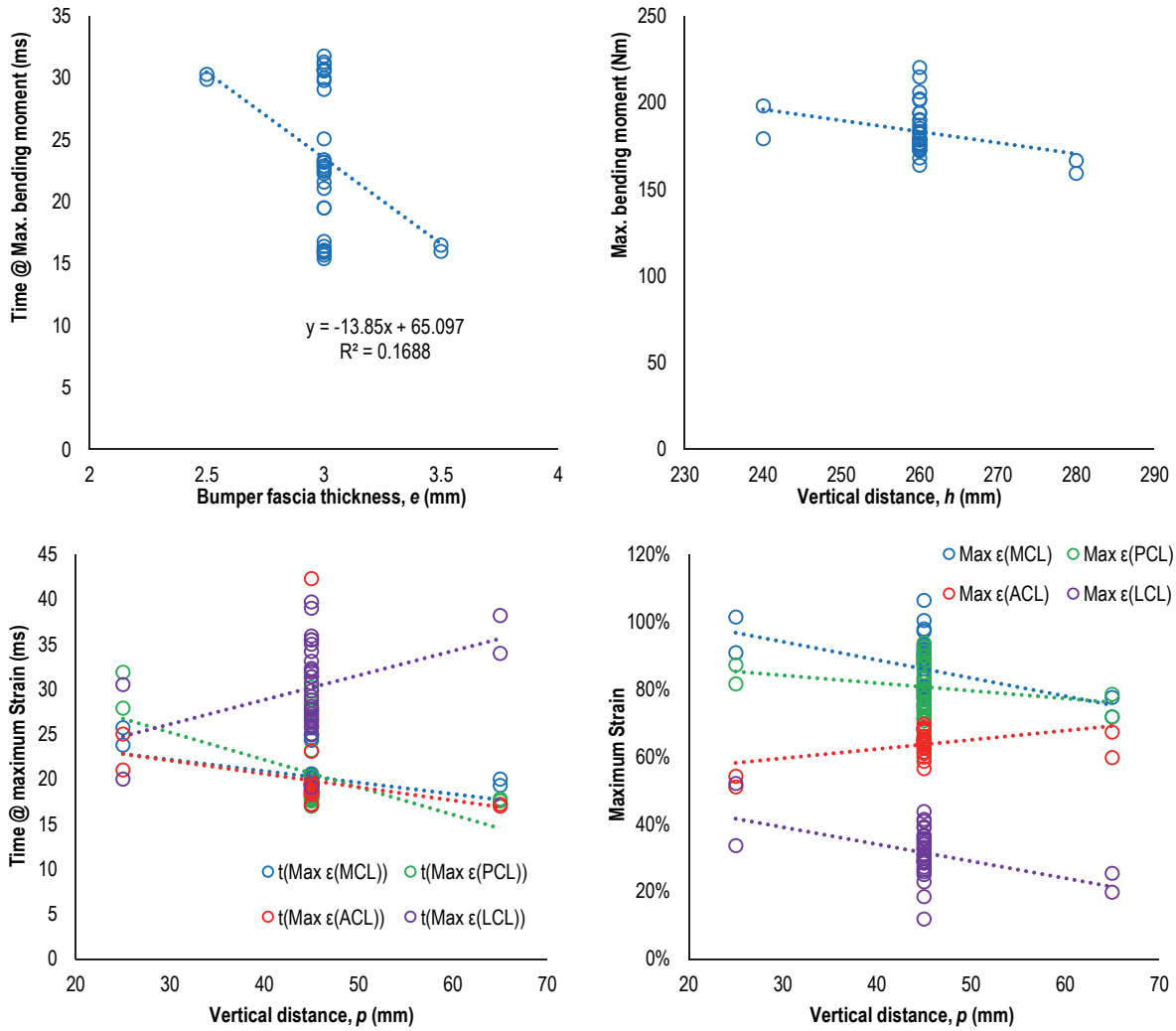


Fig. A12. Influence of the bumper fascia thickness *e* (top left hand side), of the vertical distance *h* (top right hand side) and of the vertical distance *p* (bottom row) on the outputs in terms of time corresponding to its maximum values (on the left hand side) and in terms of maximum values (on the right hand side). The maximum bending moment is considered in the topo row, the maximum ligament strains are considered in the bottom row.

Table 1. Material and geometrical parameters considered for the analysis and their variations.

.

		Levels						
		−3	**−2**	**−1**	**0**	**+1**	**+2**	**+3**
Material parameters	***e*** (mm)			2.5	3.0	3.5		
	E_h (MPa)			640	1280	1920		
	E_l (MPa)			640	1280	1920		
Geometrical parameters	***d*** (mm)	−30	−20	−10	0	+10	+20	+30
	h (mm)			240	260	280		
	p (mm)			25	45	65		

Table 2. Correlation matrix of the results in terms of time corresponding to the maximum values of the considered output results.

	Y (mm)	p (mm)	h (mm)	d (mm)	e (mm)	E_h (MPa)	E_l (MPa)	t(max M(tibia))	t(max ε(MCL))	t(max ε(PCL))	t(max ε(ACL))	t(max ε(LCL))
Y (mm)	1	0	0	0	0	0	0	0.298	-0.203	-0.389	-0.109	-0.247
p (mm)	0	1	0	0	0	0	0	0.154	-0.403	-0.479	-0.242	0.385
h (mm)	0	0	1	0	0	0	0	0.151	0.083	0.208	0.023	0.066
d (mm)	0	0	0	1	0	0	0	-0.547	-0.175	0.105	0.008	-0.140
e (mm)	0	0	0	0	1	0	0	-0.411	-0.028	0.185	-0.002	-0.075
E_h (MPa)	0	0	0	0	0	1	0	-0.178	-0.478	-0.379	-0.638	-0.302
E_l (MPa)	0	0	0	0	0	0	1	-0.214	0.079	0.151	0.018	0.043
t(max M(tibia))	0.298	0.154	0.151	-0.547	-0.411	-0.178	-0.214	1	0.084	-0.352	-0.123	0.315
t(max ε(MCL))	-0.203	-0.403	0.083	-0.175	-0.028	-0.478	0.079	0.084	1	0.549	0.565	0.290
t(max ε(PCL))	-0.389	-0.479	0.208	0.105	0.185	-0.379	0.151	-0.352	0.549	1	0.508	0.126
t(max ε(ACL))	-0.109	-0.242	0.023	0.008	-0.002	-0.638	0.018	-0.123	0.565	0.508	1	0.146
t(max ε(LCL))	-0.247	0.385	0.066	-0.140	-0.075	-0.302	0.043	0.315	0.290	0.126	0.146	1

Table 3. Correlation matrix of the results in terms of the maximum values of the considered output results.

	Y (mm)	p (mm)	h (mm)	d (mm)	e (mm)	E_h (MPa)	E_l (MPa)	max M(tibia))	max ε(MCL)	max ε(PCL)	max ε(ACL)	max ε(LCL)
Y (mm)	1	0	0	0	0	0	0	-0.112	0.492	0.692	-0.414	-0.176
p (mm)	0	1	0	0	0	0	0	-0.035	-0.424	-0.207	0.459	-0.460
h (mm)	0	0	1	0	0	0	0	-0.321	-0.112	-0.156	0.004	-0.010
d (mm)	0	0	0	1	0	0	0	-0.829	-0.679	-0.253	-0.268	-0.511
e (mm)	0	0	0	0	1	0	0	0.001	-0.039	-0.066	-0.251	-0.020
E_h (MPa)	0	0	0	0	0	1	0	0.199	-0.013	0.231	0.045	-0.044
E_l (MPa)	0	0	0	0	0	0	1	-0.037	-0.088	-0.021	0.012	0.052
max M(tibia)	-0.112	-0.035	-0.321	-0.829	0.001	0.199	-0.037	1	0.569	0.243	0.269	0.460
max ε(MCL)	0.492	-0.424	-0.112	-0.679	-0.039	-0.013	-0.088	0.569	1	0.760	-0.256	0.430
max ε(PCL)	0.692	-0.207	-0.156	-0.253	-0.066	0.231	-0.021	0.243	0.760	1	-0.299	0.112
max ε(ACL)	-0.414	0.459	0.004	-0.268	-0.251	0.045	0.012	0.269	-0.256	-0.299	1	-0.123
max ε(LCL)	-0.176	-0.460	-0.010	-0.511	-0.020	-0.044	0.052	0.460	0.430	0.112	-0.123	1